# Co-K and Mo-K edges Quick-XAS study of the sulphidation properties of Mo/Al2O3 and CoMo/Al2O3 catalysts

Amélie Rochet, Bertrand Baubet, Virginie Moizan-Baslé, Christophe Pichon, Valérie Briois

# Etude des propriétés de sulfuration de catalyseurs $Mo/Al_2O_3$ et $CoMo/Al_2O_3$ par spectroscopie d'absorption des rayons X résolue dans le temps aux seuils K du cobalt et du molybdène

# Co-K and Mo K edges Quick-XAS study of the sulphidation properties of $Mo/Al_2O_3$ and $CoMo/Al_2O_3$ catalysts

**Amélie Rochet[a,b,c,*], Bertrand Baubet[a], Virginie Moizan[a], Christophe Pichon[a], Valérie Briois[b,*]**

[a] IFP Energies nouvelles, Rond-point de l'échangeur de Solaize, BP 3, 69360 Solaize, France, 00 33 4 37 70 20 00, 00 33 4 37 70 27 45, virginie.moizan@ifpen.fr

[b] Synchrotron SOLEIL, L'Orme des Merisiers, Saint-Aubin, BP 48, 91192 Gif-sur-Yvette Cedex, France, 00 33 1 69 35 96 44, 00 33 1 69 35 94 56, valerie.briois@synchrotron-soleil.fr

[c] Laboratório Nacional de Luz Síncrotron, CEP 13083-970, Caixa Postal 6192, Campinas, São Paulo, Brazil, 00 55 19 35 17 51 80, 00 55 19 35 12 10 04, amelie.rochet@lnls.br

Abstract:

The sulphidation process of two catalysts ($Mo/Al_2O_3$ and $CoMo/Al_2O_3$) has been investigated by time-resolved X-ray Absorption Spectroscopy. With the unique edge jumping capability available at the SOLEIL synchrotron, studies of the cobalt and molybdenum species have been conducted simultaneously on the same bimetallic catalyst. A methodology combining Principal Component Analysis and Multivariate Curve Resolution with Alternating Least Squares methods unravels a 3-stepped or 4-stepped sulphidation process for the bimetallic and monometallic catalysts, respectively. An oxysulphide has been identified as intermediate for $Mo/Al_2O_3$ and a $MoS_3$-like species has been observed for both catalysts.

*KEYWORDS: hydrodesulphurisation, time-resolved XAS, chemometric methods, intermediates, $CoMo/Al_2O_3$, $Mo/Al_2O_3$*

## 1. Introduction

To improve cycle length and catalytic performances of heterogeneous catalysts a better understanding of their structure under realistic conditions is essential. X-ray absorption spectroscopy (XAS) is a powerful tool to study heterogeneous catalysts. It provides structural and chemical information about a selected element and is very effective to reveal structure-property relationships during *in situ* measurements carried out under high temperature, high pressure conditions under different atmospheres. On the one hand, through a fruitful collaboration between the French synchrotron radiation facility SOLEIL and academic (Unité de Catalyse et Chimie du Solide (Lille 1), Laboratoire de réactvité de Surface (Paris VI)) or pre-industrial (IFPEN) partners, SOLEIL's XAS beamlines are equipped with various catalytic cells and necessary devices (mass spectrometer, gas distribution rack…) for *operando* studies of catalysts [1]. On the other hand, the installation of the home-made double Quick-EXAFS monochromator [2], first installed at the SAMBA beamline [3] and now at the ROCK one, offers unique capabilities for the sub-second time-resolved characterisation of catalysts in working conditions.

The purpose of this paper is to illustrate with the study of the activation of molybdenum based catalysts used in the hydrodesulphurisation process (HDS) the methodology which is now available at SOLEIL for the time-resolved Quick-XAS study of heterogeneous catalysts.

The HDS process is an essential process [4] in the petroleum industry. It consists in the catalytic removal of the sulphur heteroelement from diesel and gasoline. Due to strengthened environment regulations, refiners have to lower the sulphur content in oil fractions by improving HDS processes. Very often, to modify the active phase performances, $MoS_2$ nanocrystallites are decorated with cobalt atoms to form the mixed CoMoS phase according to the Topsøe's model [5]. The active phase is generally obtained by sulphiding oxidic precursors during a thermal treatment under a

control $H_2S/H_2$ atmosphere. Thus monitoring the sulphidation process is crucial to better understand the formation of the active phase. Since molybdenum and its promoter are strongly linked in the reaction, studying simultaneously Mo and Co species is essential to reveal the relationship between both metals. Moreover as the sulphidation process is a dynamic process, it is crucial to use an *in situ* time-resolved technique to obtain reliable results. Herein, using Quick-XAS, we have compared the sulphidation properties of a monometallic Mo catalyst supported on $Al_2O_3$ with those of the bimetallic Co/Mo catalyst supported on the same alumina support. We used the unique possibility of the edge jumping offered by the double SOLEIL's Quick-EXAFS monochromator [2] to record data at both molybdenum and cobalt K edges (measurements on the same sample under similar conditions with a few seconds between measurements of both edges) of the bimetallic CoMo supported catalysts. It allowed a direct and unambiguous comparison of time-resolved formation of intermediate species evolving during the studied reaction.

As time-resolved techniques produce huge amount of data, resorting to chemometric tools is essential to unravel the mechanisms leading to the formation of active species. In this work we used a methodology combining Principal Component Analysis (PCA) and Multivariate Curve Resolution with Alternating Least Squares (MCR-ALS) methods to quantify and extract intermediate species for the different catalysts.

## 2. Sample preparation and *ex situ* characterisation

$CoMo/Al_2O_3$-supported catalysts were synthesized by incipient wetness impregnation of a δ-alumina support with a solution of $MoO_3$ (0.6 M) (Sigma-Aldrich) dissolved into $H_2O_2$ (3 M) in which cobalt nitrate (Prolabo) was subsequently added in the 0.5 Co/Mo ratio. The used δ-alumina carrier had a specific surface area of 143 $m^2/g$ and a pore volume of 0.99 mL/g. The monometallic $Mo/Al_2O_3$-supported catalyst was synthesized

using the same procedure without the further addition of cobalt nitrate. The loading of the monometallic catalyst is equal to the relative loading of the corresponding metal in the bimetallic catalyst (Mo: 5.5 wt.%, Co:1.5 wt.%).

Following the impregnation step, the solid was matured in a saturated water atmosphere during 12 h in order to ensure a good diffusion of the cobalt and molybdenum precursors into the alumina porosity. Then a drying step at 120°C overnight in a static air oven was carried out to obtain the dried $Mo/Al_2O_3$ and $CoMo/Al_2O_3$ oxidic precursors.

These as-prepared catalysts are characterised by Raman spectroscopy in the 450-1200 $cm^{-1}$ range with a Kosi (Kaiser Optical Systems Incorporation) RXN1 spectrometer using a 785 nm laser diode as the excitation source with a laser power at the sample position of about 2 to 10 mW and coupled to an optical microscope (X10 magnification). Several positions over the surface of the catalysts were measured in order to check the homogeneity of the species dispersed at the surface of the support. The spectra acquisition consisted of several accumulations of 900s each at a resolution of 2 $cm^{-1}$.

## 3. *In situ* measurements

### 3.1. *In situ* treatment

Both Mo and CoMo supported catalysts were sulphided *in situ* during synchrotron measurements. For this purpose, the powdery sample was loaded in the transmission cell available at the hard X-rays SAMBA beamline (Figure 1). Technical details of the cell are presented in 3.3 of a previous work [1c].

When Mo and Co K edges are investigated on the same sample, a compromise has to be done concerning the sample absorption at both edges. To achieve the desired sample absorption the cavity of the sample holder was filled with 90 mg of the powdery

catalyst premixed with about 220 mg of diamond powder. We obtained an edge jump around 0.3 at the Mo K edge and an edge jump around 0.5 at the Co K edge.

A thermal treatment of 2℃/min from RT to 400℃ und er a flow of a mixture of 15% of $H_2S$ into $H_2$ at atmospheric pressure followed by a plateau of 2 h (with 3 mL/min controlled by Brooks mass flow controllers), has been used to study the sulphidation process under relevant conditions.

### 3.2. On-line Raman spectroscopy of gas products

The gases at the cell outlet were analysed by Raman spectroscopy before being treated by the exhaust removal gas system equipping the beamline. A 532 nm Raman spectrometer (Kaiser Optical Systems Incorporation, KOSI RXN1 type) equipped with a Raman probe mounted at the cell outlet using Swagelok fittings was used (Figure 1). Mainly the area of the Raman bands characteristic of $H_2$ located at 588 $cm^{-1}$ (area between 572 - 604 $cm^{-1}$) and $H_2S$ located at 2611 $cm^{-1}$ (area ranged between 2599 – 2625 $cm^{-1}$) (Figure S 1 in supporting information) were monitored using the Holoreact software developed by KOSI allowing to obtain the profile of those reactants during the whole *in situ* treatment.

### 3.3. XAS measurement

First, data of the fresh oxidic precursors were collected. Then the samples were sulphided *in situ* during the data collection. XAS spectra were acquired in transmission mode with three Ohken ionisation chambers (IC) as X-rays detectors. During the experiment, the ICs were filled with argon for measurements at the Mo K edge and with nitrogen for those at the Co K edge. The Mo K edge XAS spectra were acquired with the Si311 channel-crystal tuned to a Bragg angle of 10.8° and a crystal oscillation amplitude of 0.7° around this value was chosen to a cquire an entire EXAFS (Extended X-ray Absorption Fine Structure). For the Co K edge measurements, the Si111 channel-

cut crystal was tuned to a Bragg angle of 13.4° and a crystal oscillation amplitude of 2.2° was used. For each edge a frequency of 1 Hz was selected for the crystal oscillation allowing the measurement of two spectra each second (one with increasing energies, the other one with decreasing energies). The collimating and focusing cylindrically bent Pd coated mirrors were aligned with a grazing incidence of 3.1 mrad at both edges.

Both Co and Mo edges of the bimetallic catalyst have been alternatively characterised during the same *in situ* treatment thanks to the edge jumping capability [2] of the SAMBA beamline [3]. The sequence of acquisition used in this work is presented in Figure 2.

Si111 and Si311 channel-cut crystals were alternatively used (every 65 s) as monochromator for the Co and Mo K edges. Thus the temperature difference between Co and Mo successive measurements was of about 4°C (heating rate at 2°C/min). Consecutive spectra saved during one minute at each edge were merged to improve the signal-to-noise ratio. Thanks to the beamline automation, the amplifier gains and the gaseous content of the ICs were changed while the monochromator setup was changed.

## 4. Methodology of time-resolved XAS analysis to reveal intermediates species

### 4.1. XAS analysis

Analysis of the X-ray Absorption Near Edge Structure (XANES) data was performed by using the Athena graphical interface program [6]. The energy was calibrated to the first inflection point of a Co or Mo metal foil defined at 7709 eV and 20003.9 eV, respectively. Then the spectra were background corrected and normalised using the flattening algorithm used by Athena [6].

Fits of EXAFS spectra were performed by using the Artemis graphical interface program [6]. Quick-XAS spectra of standard references prepared as pellets were

recorded at Room Temperature (RT) at both edges in order to check the transferability of *ab initio* phase and amplitude functions calculated by the FeFF6 code [7]. Structural parameters R (average atomic distance from the absorbing atom), N (coordination number) and σ (Debye-Waller factor) were determined by least-square fitting procedures using a multiple k-weight data procedure. The goodness of fit is given by the minimum value of the statistical $\chi^2$ metric parameter and of the reduced $\chi^2_\nu$ quality factor defined as the ratio of $\chi^2$ over $\upsilon$ where $\upsilon = N_{ind} - N_{var}$ with $N_{ind}$ the number of free parameters allowed to vary in a fit and $N_{var}$ the number of variables used in the model (as defined by the IXS standards and criteria committee and available at http://ixs.iit.edu/subcommittee_reports/sc/err-rep.pdf). The $\chi^2_\nu$ parameter obtained for each fit and the $R_F$-factor, which measures the relative misfit with respect to the experimental data, are reported in the tables.

### 4.2. Quantification of number of intermediate species and identification by chemometric methods

During the sulphidation process, complex chemical transformations involving several intermediate species occur. The determination of the number of those intermediate species cannot be easily done by lonely visualising the XANES spectra. Even if the observation of isosbestic points is a good tool to estimate the number of intermediate species and their existence domain upon time (or temperature changes), this by-eye inspection does not guarantee the purity of the observed pivotal spectra. Furthermore, the co-existence of several intermediate species often precludes them for being distinguished due to the presence of several set of isosbestic points. Actually, as used in several recent time-resolved XANES studies [8], more sophisticated multivariate methods based on linear algebra could be used to estimate the number of components in a mixture of unknowns involved in a reaction. One can also extract their pure spectra and provide a quantitative concentration profile for each component. The key ideas of

those methods are to represent the original data matrix *D* containing the q spectra recorded along the reaction with a k number of energy points by the sum of a product of two matrices *C* and $S^T$ characterised for each matrix in one direction by a smaller n dimensionality than q and of a residual matrix *E* containing the experimental noise, as schematised Figure 3.

In the Principal Component Analysis (PCA) approach, the row-vectors corresponding to the absorbance of the set of data are represented mathematically as a linear sum of a minimum set of uncorrelated row-vectors $S^T$ called principal components weighted by the proportion of this component loaded in the column vector *C*. Such a PCA analysis is possible if the number of spectra is larger than the number of the components. Every component makes a maximum contribution to the sum of the variances of the variable under the constraint that each component is orthogonal to the preceding components. Each orthogonal PCA component is associated with an eigenvalue which is used to sort the components by the amount of variance explained. Thus, PCA allows reducing a large set of data to a controllable set of spectra. It is noteworthy that the set of PCA components so-determined are not spectra of chemical species. The identification of chemical species involved in the *D* matrix data set can be obtained through the so-called target transformation method as explained in [9]. This requires that the XAS spectrum of the chemical species submitted to the target transformation test has been already experimentally measured.

The so-called Multivariate Curve Regression-Alternating Least Square (MCR-ALS) iterative method will provide a meaningful estimation of *C* and $S^T$ in which those matrices take a chemical signification: for the $i^{th}$ column vector of *C* the profile of concentration of the $i^{th}$ chemical species described by its pure spectrum represented by the $i^{th}$ row-vector of $S^T$. Such decomposition into meaningful matrices is in the case of the absorption spectroscopy a transcription of the Beer-Lambert relation at which the XAS spectroscopy obeys. The convergence of the MCR-ALS algorithm towards *C* and

$S^T$ matrices is greatly helped by the use of physically meaningful constraints such as the non-negativity of both concentration and absorbance spectrum, the closure and/or unimodality of concentrations. It means that the sum of concentrations (proportion of species) is equal to the total concentration of absorbing atom (100%) and that only one maximum can describe the concentration profiles of the species. The number of n components which has to be used as starting guess of the iterative fitting has to be determined before starting the regression, using for instance PCA. The MCR-ALS methodology applied to XAS can be found in more details in [8d] and [10].

The use of those chemometric methods for the determination of speciation (concentration profiles and pure spectra) by Quick-XAS upon monitoring of reaction is nowadays the indispensable method to handle the huge amount of data that a Quick-XAS beamline delivers for several hours of kinetics. It's the reason why we note a remarkable increase of recent publications using such methods in different scientific fields as energy storage, catalysis, materials and environmental sciences [8c, d], [10] and [11]. Both methods will be herein illustrated with the Mo speciation of the $Mo/Al_2O_3$ and bimetallic $CoMo/Al_2O_3$ catalysts. We used the Matlab® platform (R2011b) to carry out PCA of the normalised Quick-XAS spectra at the Mo K edge to determine the minimal number of components [12] required to satisfactorily reproduce the set of experimental molybdenum XAS data. In that case, the Matlab script for PCA analysis described in [13] was used. We also performed PCA on the first derivative of the Quick-XAS data. No PCA has been used for the Co K edge data since no evidence of intermediate species has been observed. The MCR-ALS fitting on the Quick-XAS data was carried out using the als2004 toolbox developed by the group of Roma Tauler [14] on the Matlab® plateform.

The first sixth PCA components obtained for the $CoMo/Al_2O_3$ catalyst are presented as example in Figure 4. The distinction between the components describing the data set and those which are related to experimental noise can be done using the so-called

scree plot which displays the successive eigenvalues ordered by diminishing value against the number of the corresponding component. A break of the slope of this scree plot is usually ascribed as the minimum number of components to consider in the system. Such scree plots obtained on the XAS data set and their corresponding derivative are represented in Figure 5 for both catalysts considering the first 10 components. The log-scale representation of the eigenvalues extracted from the PCA is sometimes more convenient than the traditional scree plot to better visualise the first break slope in the variation of eigenvalues as a function of component numbers. Then, on Figure 5, the scree plot obtained from PCA performed on the XAS data is presented on a log scale (left) whereas the one obtained with the PCA on derivatives is presented with a linear scale (right). Both representations of the same data set (XAS and derivative) lead to the same conclusion with a break slope occurring at the third and fourth components for the $CoMo/Al_2O_3$ catalyst and $Mo/Al_2O_3$ catalyst, respectively. It is noteworthy that similarly to the scree plot, a variance plot in which the explained variance considering the successive component can be plotted as a function of the number of components. In that case, it is more convenient to use the variance information extracted from the analysis of the derivatives rather than the XAS data. Indeed, the change of explained variance observed considering the successive components in the PCA analysis of derivatives appears more discriminating than the change reported for the PCA analysis of XAS. This behaviour results from the peculiar shape of normalised XAS data. The first PCA component is essentially the average of all the sample data and then leads to more than 99% of explained variance. The others PCA components account for the small fluctuations between the experimental spectra (as shown in Figure 4). At the opposite, the derivative spectra with positive and negative peaks moving in energy position depending of the species oxidation state lead to PCA components with marked increase of explained variance when considering successive PCA. For instance for the $Mo/Al_2O_3$ catalyst, the first component obtained from derivative analysis explains 82.85% of variance, the second explains some more

14.41% and the two other components 1.40 and 0.15%, respectively. The fifth component and the next ones allow for explaining only 0.05% and less than 0.04% of additional variance which becomes significantly too small to be considered as correlated in the information contained in the *D* matrix and should remain in the *E* matrix corresponding to the noise (see Figure 3).

The respective rank orders obtained by PCA analysis are then used for the MCR-ALS analysis of data set related to both catalysts. For the minimisation, the used constraints were the non-negativity of both absorption and concentration, the closure condition for the concentrations and the unimodality for the concentrations during the entire sulphidation process.

## 5. Results and discussion

### 5.1. Structure of the oxidic precursors

Both dried oxidic catalysts were at first characterised as prepared before any treatment. Figure 6 compares the Raman data recorded for the as-prepared dried catalysts. For the monometallic $Mo/Al_2O_3$ catalyst, only the data recorded in the 750-1050 $cm^{-1}$ are presented because a strong fluorescence background measured for this sample below 700 $cm^{-1}$ hinders to resolve lines with small intensity (insert in Figure 6 (A)). The 800-1000 $cm^{-1}$ Raman shift range is informative on the oxygen-molybdenum stretching vibrations of polyoxomolybdates. Whatever the Regions of Interest (ROIs) investigated for the $Mo/Al_2O_3$ catalyst, a broad band is obtained with the emergence of defined peaks at 944, 902, 878 $cm^{-1}$ and a shoulder at 850 $cm^{-1}$. This peculiar shape suggests the overlap of broad lines characteristic of different molybdenum based species.

At the opposite, the spectra recorded for the bimetallic $CoMo/Al_2O_3$ catalyst at different ROIs display well-defined lines in the Raman shift below 700 $cm^{-1}$ and well-shaped

lines in the 800-1000 $cm^{-1}$ together with the characteristic symmetric stretching vibrational mode of the nitrate anions introduced with the promoter at 1050 $cm^{-1}$ (Figure 6 (B)). Some of the lines are clearly consistent with the formation of $Co_3O_4$ (lines at 693, 621 and 485 $cm^{-1}$ [15] whereas the other lines at 683, 614, 518 and 477 $cm^{-1}$ are assigned to the formation of the $CoAl_2O_4$ spinel aluminate [16].

On both catalysts, but mainly on the $Mo/Al_2O_3$ one, the lines at 944, 900 $cm^{-1}$ and the tail toward 850 $cm^{-1}$ could be ascribed to the presence of heptamolybdate and molybdate species in interaction with the support [17].

The well-shaped lines with intensity maximum moving from 936 to 955 $cm^{-1}$ clearly observed on the $CoMo/A_{l2}O_3$ catalysts are the characteristic fingerprints of different polyoxomolybdate species dispersed at the surface of the support. The presence of the intense line at 950-955 $cm^{-1}$ with a shoulder at 902 $cm^{-1}$ (ROI1 and ROI2) could be tentatively ascribed to the precipitation of the 6-molybdoaluminate Anderson-type heteropolyanion $(AlMo_6O_{24}H_6)^{3-}$ (also referred as $AlMo_6$) [18]. The lines peaking at lower Raman shift positions (936-940 $cm^{-1}$) could result from the precipitation of heptamolybdate species [18]. These findings point out that in agreement with the previous observations reported in the literature [19], $CoMo/Al_2O_3$ catalysts are complex materials with dispersion of various cobalt and molybdenum-based species.

The Mo K edge XANES and EXAFS spectra and corresponding Fourier transforms (FT) of the dried catalysts are compared Figure 7 to those of selected references such as $AlMo_6$ (with ammonium as counter-anion), AHM (ammonium heptamolybdate $(NH_4)_6[Mo_7O_{24}]$) and the dimeric molybdate compound $(NH_4)_2[Mo_2O_7]$. For all the samples, an intense pre-edge peak on the XANES data is observed (Figure 7 (A)). It arises from transition from 1s towards molecular orbitals in which 4d Mo orbitals are hybridised with p Mo orbitals due to the presence of a non-centrosymmetric environment for Mo [20]. Less centrosymmetric is the environment, more intense is the

pre-edge peak as clearly observed comparing the pre-edge feature of the corner sharing tetrahedrons of the dimeric $(NH_4)_2[Mo_2O_7]$ molybdate reference and those of the more centrosymmetric AHM or $AlMo_6$ references. A quite similar shape of XANES spectra is observed for both catalysts with nevertheless a slight intensity increase of the pre-edge feature and bump located at 20044 eV for the $Mo/Al_2O_3$ sample compared to the $CoMo/Al_2O_3$ one. These features are related to the presence of tetrahedral molybdate species [21] in agreement with the previously discussed Raman results.

Both $Mo/Al_2O_3$ and $CoMo/Al_2O_3$ catalysts EXAFS data and their corresponding FT display significant differences (Figure 7 (B) and (C)). It is important to note the in-phase shape of the EXAFS oscillations and corresponding FT of the $CoMo/Al_2O_3$ catalyst and $AlMo_6$ reference in agreement with the presence of the Anderson-type heteropolyanion (HPA) suggested by Raman. Such observation has been already done in the case of dried NiMo catalysts supported on alumina and prepared by a similar method [22].

These qualitative descriptions for both catalysts are confirmed by the structural parameters determined by the EXAFS fits presented in Table 1 (and Figure S 2 in supporting information). A large distribution of Mo-O distances are found in the first coordination shell in agreement with a non-centrosymmetric environment for Mo whereas the presence of a Mo-Al contribution at 3.40 (0.05) Å for fitting the catalysts is in good agreement with the dispersion of the $AlMo_6$ at the surface of alumina. It is noteworthy, that the presence of a Mo-Al path contribution at 2.65 (0.05) Å is required to get the best fit for both catalysts. Such a contribution might be due to interactions between the support and Mo species, as already noted for dried NiMo catalysts supported on alumina [22].

Table 1: Parameters obtained from the fit of the Mo K edge EXAFS spectra of the oxidic bimetallic CoMo and monometallic Mo supported catalysts at the Mo K edge ($\Delta k$ = 3.5-12.5 $Å^{-1}$, $S_0^2$ =0.96, $E_0 + \Delta E$ = 20019.4 eV).

| Backscatterer | N | R (Å) | $\sigma^2$ (Å$^2$) x $10^{-3}$ | R-factor | $\chi^2_\nu$ |
|---|---|---|---|---|---|
| ***Fresh dried CoMo (RT)*** | | | | | |
| O | 3.1 ± 0.8 | 1.74 ± 0.01 | 3.6 ± 2.0 | 0.0031 | 76 |
| O | 1.7 ± 0.7 | 1.96 ± 0.03 | | | |
| O | 0.5 ± 0.6 | 2.29 ± 0.07 | | | |
| Al | 0.5 ± 0.3 | 2.65 ± 0.05 | | | |
| Mo | 0.6 ± 0.6 | 3.34 ± 0.04 | | | |
| Al | 1.2 ± 0.8 | 3.39 ± 0.06 | | | |
| ***Fresh dried Mo (RT)*** | | | | | |
| O | 3.4 ± 0.5 | 1.75 ± 0.01 | 4.6 ± 2.0 | 0.0021 | 66 |
| O | 1.5 ± 0.4 | 1.97 ± 0.02 | | | |
| O | 0.3 ± 0.4 | 2.26 ± 0.06 | | | |
| Al | 0.6 ± 0.2 | 2.65 ± 0.05 | | | |
| Mo | 0.3 ± 0.4 | 3.31 ± 0.08 | | | |
| Al | 1.1 ± 0.4 | 3.38 ± 0.03 | | | |

Due to the strong differences in the shape of EXAFS oscillations of both catalysts and references (Figure 7 (B)), we tentatively fit by a least square minimisation the EXAFS spectra of catalysts using linear combination fittings (LCF) of reference EXAFS data. Even if such linear combinations must be taken with care due to the fact that we are building EXAFS spectra of dispersed species in interaction with the support with those of bulk ones; the results give insights about the mixtures of molybdenum species at the surface of the support.

Table 2: Results of the linear combination fittings of Mo K edge EXAFS spectra of the oxidic bimetallic CoMo and monometallic Mo supported catalysts.

| Sample | $AlMo_6$ | $(NH_4)_2[Mo_2O_7]$ | AHM | R-factor | $\chi^2_\nu$ |
|---|---|---|---|---|---|
| **CoMo catalyst** | 58.7 % | 26.6 % | 14.7 % | 0.08346 | 0.31251 |
| **Mo catalyst** | 35.8 % | 47.2 % | 17.0 % | 0.02851 | 0.08799 |

Table 2 gathers the results of the linear combinations presented Figure 8. The striking conclusion is the dominant presence of $AlMo_6$ HPA and molybdate-based species for the $CoMo/Al_2O_3$ catalyst and for the $Mo/Al_2O_3$ catalyst, respectively. It is noteworthy that such proportions are in agreement with the Raman discussion presented herein.

The data measured at the Co K edge for the CoMo bimetallic supported catalyst are presented on Figure 9 and compared to the ones of the $Co_3O_4$ and $Co(NO_3)_2{\cdot}6H_2O$ references. The shape of the XANES spectrum of the CoMo sample is close to the one of the cobalt nitrate but not perfectly stackable suggesting that the local order around Co in the catalyst is different from the one characterising the solid $Co(NO_3)_2{\cdot}6H_2O$ reference. On the Fourier transform, the $CoMo/Al_2O_3$ catalyst presents only one main contribution around 1.5 Å (not phase shift corrected). It corresponds to well dispersed oxidic Co species at the surface of the alumina support. The characteristic shape of the white line and its position in energy suggests the presence of octahedral divalent cobalt species that is confirmed by the EXAFS fitting results with 6.1 (1.3) oxygen neighbours at 2.05 (0.05) Å (RF = 0.01826, $\chi^2_\nu$ = 219). The dispersion of $Co_3O_4$ pointed out by its characteristic Raman lines for some of the ROIs on the bimetallic sample (Figure 6) is not confirmed by the XAS results. Actually as $Co_3O_4$ is a strong Raman backscatter, it can give a strong Raman signal for concentrations which are not detectable by XAS data measured in transmission mode.

### 5.2. Identification of species involved during sulphidation of oxidic precursors

The monitoring of the sulphidation process for both dried $Mo/Al_2O_3$ and $CoMo/Al_2O_3$ samples is presented in Figure 10. Figure 10 (A) and (B) correspond to the data measured at the Mo K edge for the respective catalysts whereas Figure 10 (C) displays the data measured at the Co K edge for the bimetallic catalyst. While the first spectrum (black) is the fresh sample, the others are obtained during the increasing time (*i.e.* increasing temperature) upon treatment under $H_2S/H_2$. During the plateau at 400℃, the shape of the Mo K edge XAS spectra of both catalysts is similar to the spectrum of $MoS_2$. Since for the bimetallic catalyst, the XAS measurements have been done with the edge jumping mode, less spectra at the Mo K edge has been recorded compared to the ones of the pure Mo sample. For both catalysts, the change in the

shape of the Mo K edge XANES spectra with the disappearance of the pre-edge feature and the shift at lower energy of the rising edge are characteristic of an exchange of oxygen ligands by sulphur ones accompanied by a reduction of the Mo oxidation state.

The Co K edge XANES spectra present a decrease of the white line intensity with increasing temperature (Figure 10 (C)). At the end of the sulphiding treatment, the white line totally disappears, as already observed in other works for sulphided cobalt species [23].

The moduli of the Mo K edge Fourier transforms obtained during the sulphidation process are presented on Figure 11 for the bimetallic and monometallic catalysts.

On Figure 11 (top), the effect of the sulphidation is observed around 75℃ when the signal centred around 1.2 Å disappears and a contribution around 1.9 Å appears (not phase shift corrected). This new signal has been already observed by Nicosia *et al.* [23] and has been attributed to the Mo-S contribution of a $MoS_3$-like species. The shoulder around 2.4 Å could be attributed to the Mo-Mo contribution as observed in other works [23] and [24]. It is noteworthy that the intensity of this contribution centred around 1.9 Å is increasing with the temperature. At 237℃, the Mo-S contribution is shifted toward lower distances (centred on 1.8 Å, not phase shift corrected) and just after this fast change, a new contribution around 2.8 Å is appearing. Those contributions are attributed to Mo-S and Mo-Mo signals of $MoS_2$, respectively. The amplitude of the Mo-S and Mo-Mo contributions increases with increasing temperature, showing the growth of the $MoS_2$ crystallites (Figure 11, top).

Thus for the bimetallic CoMo catalyst, as already observed for other works [23], the sulphidation of the molybdenum species seems being composed of three stages, roughly marked on the Fourier Transforms by the different colors.

For the monometallic catalyst (Figure 11, bottom), the molybdenum environment is affected by the sulphiding treatment at lower temperature (~35℃) compared to the bimetallic sample. Besides to the broad contribution corresponding to the first oxygen coordination shell, a new contribution located around 2.1 Å (not phase shift corrected) can be observed at temperature below 50℃. Between 50 and 200℃, one can see a strong contribution centred at 2.0 Å (not phase shift corrected). The intensity of this contribution increases up to 111℃ while the Mo-O signal disappears. While the temperature keeps increasing, the intensity of this contribution located at 2.0 Å decreases and the peak continuously shifts towards lower distances up to 1.8 Å (not phase shift corrected). Then this distance value remains constant until the end of the treatment. It corresponds, as for the bimetallic $CoMo/Al_2O_3$ catalyst, to the distance of the first coordination shell in the $MoS_2$ crystallites. Simultaneously a contribution around 2.8 Å, attributed to Mo-Mo signals of $MoS_2$ appears. As observed for the bimetallic catalyst, the amplitude of the Mo-S and Mo-Mo contributions get stronger with increasing temperature, showing again the growth of the $MoS_2$ crystallites during the last period of the heating ramp.

Thus for the monometallic Mo catalyst, the sulphidation process seems being composed of four stages contrary to the three ones previously observed for the bimetallic sample.

The structure of the pivotal species involved in the 3 or 4 stages characterising the sulphidation of the bimetallic and monometallic catalysts were then analysed in-depth thanks to the MCR-ALS method applied on the respective data set. It is noteworthy that the optimal number of PCA components allowing to describe the time-resolved data set collected during sulphidation and discussed previously in the experimental section is equal to the number of distinct stages evidenced by the qualitative analysis of the Fourier transforms changes.

According to the matrix rank previously determined by PCA, the MCR-ALS minimisation for the $CoMo/Al_2O_3$ catalyst was done with three components. The obtained spectra corresponding to these pure components are presented Figure 12 and named hereafter *MoCo-comp.1*, *MoCo-comp.2* and *MoCo-comp.3*. For the monometallic $Mo/Al_2O_3$ catalyst, the matrix rank for the MCR-ALS was set to 4 and the four identified species, named hereafter *Mo-comp.1*, *Mo-comp.2*, *Mo-comp.3* and *Mo-comp.4*, are presented Figure 13.

The spectra of the first and last components determined by MCR-ALS for each catalyst are superimposable to the respective oxidic precursors and fully sulphided catalysts (as presented in supporting information, Figure S 3). It is noteworthy that the oxidic precursors have been identified as a mixture of HPA and molybdate-based species. However the chemometric methods used herein, identify only one component for this initial state. This strongly suggests that the initial phases are concurrently transformed in a same manner.

The XANES spectra obtained for the *MoCo-comp.2* species and for the *Mo-comp.3* species do not display the pre-edge feature characteristic of oxidic species presenting a non-centrosymmetrical environment around Mo. This feature suggests that those species are fully sulphided species. Actually the spectrum of *MoCo-comp.2* is similar to the one published in [25] for the amorphous $MoS_3$ compound whereas the faintly marked shoulder at the top of the rising edge observed for the *Mo-comp.3* seems to be a fingerprint of the $MoS_6$ phase [25] prepared from oxidation by iodine of a solution of ammonium thiodimolybdate ($(NH_4)_2Mo_2S_{12}$) [26]. The structure of the later phase is similar to the one of $MoS_3$ but containing more abundant S-S bonds [26]. The XANES spectrum of the *Mo-comp.2* species is at the opposite characterised by a pre-edge feature shifted by ~1.8 eV to lower energies compared to the one of the first component *Mo-comp.1* (as emphasized in supporting information, Figure S 4)

suggesting the formation of oxysulphide molybdenum-based species [27]. As a matter of fact, Mo K edge spectra of some molybdenum sulphite oxidase species recently reported in the literature [28] display XANES and EXAFS features similar to the one reported for *Mo-comp.2* in which terminal oxo ligand and disulphure ligand are bonded to Mo at 1.7 Å and 2.4 Å, respectively.

The MCR-ALS determination of the spectra of pure species over the full collected energy range of the experiment allows us to treat them as a conventional absorption spectrum and then extract their EXAFS spectra and corresponding Fourier transforms as we did it with raw experimental data. The EXAFS spectra obtained from MCR-ALS and corresponding FT for both catalysts are presented on Figure 12 (B-C) and Figure 13 (B-C).

Results of the least square fittings of the EXAFS spectra for *Mo-comp.3* and *MoCo-comp.2* are presented in Table 3 and supporting information (Figure S 5 and Figure S 6).

As suggested by the qualitative analysis of the XANES, the structural parameters determined by least square fitting procedure for the *Mo-comp.3* species fully confirm the formation of $MoS_3$-like species at this stage of the sulphidation process with the characteristic Mo-Mo distance around 2.80 Å [26] and [29]. Nevertheless, as our analysis is centred on the local order around molybdenum, the distances found for the first sulphur coordination shell of Mo does not allow us to conclude on the enrichment of disulphide ligands for *Mo-comp.3* compared to $MoS_3$ as suggested with the comparison of XANES spectra reported in the literature [25].

The best fit of the *MoCo-comp.2* EXAFS data is also based on a Mo-S first coordination shell at 2.46 (0.01) Å. The fitting of the contribution at longer distances is less straightforward. As expected for $MoS_3$ a contribution of 2 Mo neighbours at 2.79 Å has been considered but does not satisfactorily reproduced the signal centred at 3 Å. Adding a refined contribution of 1 Al neighbour located around 3.41 Å, also observed

on the pristine $AlMo_6$ HPA phase, improves the fit result. However due to out-phase shift of the Mo-Mo and Mo-Al contributions, their simultaneous refinement is not allowed. Then, we limit the description of the local order around Mo for this intermediate species to the first coordination shell (Table 3 and Figure S 6, supporting information). Hereafter those components will be presented as $MoS_3$-like species.

Finally, as suggested by the closeness of the spectrum recorded for *Mo-comp.2* and the spectra reported in the literature for sulphite oxidase of molybdenum [27], this component is satisfactorily described by a mixed O and S coordination shell at distance of 1.68 Å and 2.41 Å, respectively together with a Mo-Mo contribution at 2.86 Å (Table 3 and Figure S 5 in supporting information). Such Mo-Mo distances at ~2.85 Å are commonly found in pentavalent molybdenum oxysulphides [30]. It is noteworthy that Mo-S distances at 2.40-2.45 Å are characteristic of sulphide bridging ligands but also of disulphide chelating ligands. Unfortunately, due to the lack of complementary information about the nature of sulphur ligands, the structure of the *Mo-Comp.2* species at this stage of our study cannot be more detailed.

Table 3: Parameters obtained from the fit of the Mo K edge EXAFS spectra determined by MCR-ALS for the pure intermediate species involved during sulphidation of both mono and bimetallic supported catalysts (Δk = 3.5-12.2 $Å^{-1}$ for *Mo-comp.2* and Δk = 2.3-10.0 $Å^{-1}$ for *Mo-comp.3* and *MoCo-comp.2*, $S_0^2$ =0.94, $E_0$ = 20012.2 ± 1.2 eV).

| **Backscatterer** | **N** | **R (Å)** | **$\sigma^2$ (Å²) x $10^{-3}$** | **R-factor** | **$\chi^2_\nu$** |
|---|---|---|---|---|---|
| | | ***Mo-comp.2*** | | | |
| O | 1.0 ± 0.7 | 1.68 ± 0.02 | 4.4 ± 8.7 | 0.0033 | 698 |
| S | 4.1 ± 1.0 | 2.40 ± 0.01 | 6.7 ± 3.0 | | |
| Mo | 0.5 ± 0.8 | 2.86 ± 0.03 | 0.4 ± 9.0 | | |
| | | ***Mo-comp.3*** | | | |
| S | 4.8 ± 0.6 | 2.39 ± 0.01 | 12.2 ± 1.9 | 0.0059 | 471 |
| Mo | 1.7 ± 0.7 | 2.79 ± 0.03 | | | |
| | | ***MoCo-comp.2*** | | | |
| S | 5.6 ± 0.8 | 2.46 ± 0.01 | 12.3 ± 2.3 | 0.0063 | 265 |

### 5.3. Evolving profile concentration of metallic species and reactants upon sulphidation

Besides the determination of the pure spectra of intermediates species involved during the sulphidation processes of both catalysts, the MCR-ALS methodology directly provides the concentration profile of those species upon reaction. The concentration profiles so-obtained are presented Figure 14 and compared to the gas profile (bottom) simultaneously monitored by TPS (Temperature Programmed Sulphidation)-Raman spectroscopy.

For the monometallic sample, the intermediate oxysulphide Mo species (*Mo-comp.2*) appears as soon as the temperature starts to increase (Figure 14 (A)) and its concentration reaches a maximum at ~55℃. At this temperature, the intermediate species (*Mo-comp.3*) identified as $MoS_6$, a $MoS_3$-like phase enriched in disulphide bonds [25, 26], starts to be formed whereas a small amount of the initial oxidic precursor (5%) is still observed and remains present up to ~200℃. Contrary to the fast transformation of *Mo-comp.1* to *Mo-comp.2, i.e.* from the oxidic precursor into the oxysulphide species, the transformation of *Mo-comp.2* to *Mo-comp.3* is slow with a temperature ranging from 55℃ to 230℃. Then it is only at this temperature that the final $MoS_2$ species appears, by transformation of $MoS_6$ into $MoS_2$. It is noteworthy that this last step in the sulphidation process of the Mo catalyst occurs only after the total transformation of the oxidic precursor into sulphided species.

For the bimetallic catalyst, the sulphidation behaviour is different (Figure 14 (B). Only three molybdenum-based species have been revealed by chemometric methods. The formation of the species identified as $MoS_3$ and the final $MoS_2$ phases starts from room temperature and around 50℃, respectively with a quite similar formation rate. But when the proportion of $MoS_3$ like species (*MoCo-comp.2*) is still increasing above 80℃, the one of the $MoS_2$ species (*MoCo-comp.3*) becomes constant up to ~200℃. At the end of this plateau (~200℃), while the initial oxidic precursor is almost vanished,

the transformation of $MoS_3$ into $MoS_2$ occurs. For the Co species, only two species were evidenced during the monitoring of the sulphidation: the oxidic precursor and the final sulphided species. As for the first transformation of the Mo-based oxidic precursor into $MoS_3$, the transformation of the oxidic cobalt species into the final one starts around room temperature. The transformation of the Co oxidic species (1.74%/℃) is slightly faster than the one of Mo (1.43%/℃) at the early stage of the heating (T<50℃). It is noteworthy that about 20-25% of molybdenum and cobalt species are concomitantly sulphided between 28 and 42℃. Then at the $MoS_2$ formation onset, the sulphidation of cobalt and molybdenum species slows down with a conversion rate of 0.78%/℃ and 0.53%/℃ (for $MoS_3$), respectively. It is worth to note that at the early stage of formation of $MoS_2$ (up to 77℃), about 14-19% of molybdenum and cobalt species are also concomitantly sulphided. At 80℃, more than 95% of sulphided cobalt and molybdenum species are present. Above this temperature the transformation of the 5 remaining per cent of cobalt species is slow with a conversion rate of 0.02%/℃. It is noteworthy that the plateau of concentration observed for cobalt species starts at the same temperature than the one observed for the final species *MoCo-comp.3*. It is recognised that the order of occurrence of formation of sulphide species is of paramount importance to lead to the formation of the CoMoS active species in which Co is decorating the edges of $MoS_2$. The sulphidation of molybdenum species, and, in particular the formation of $MoS_2$, should be concomitant or posterior to the sulphidation of cobalt species to make possible the interaction of Mo sulphide species with Co ones. Herein, the simultaneous characterisation of sulphidation of both metals unambiguously evidences that a concomitant sulphidation of Mo and its promoter occurs for about 40% of both metals. Then we can infer that a part or all of those 40% of metals leads to the formation of the active CoMoS species.

For each catalyst, the gas profile obtained by TPS-Raman spectroscopy presents the change in $H_2S$ concentration in the effluent stream of the reactor (lower black signal) and the change in the $H_2$ signal (upper red curve). A negative peak corresponds to

consumption and a positive peak to production of either $H_2S$ or $H_2$. As before the circulation of $H_2S/H_2$ a short portion of gas lines at the cell inlet and outlet are filled with nitrogen, the change in gas concentration observed at the lowest temperatures is partly due to a dilution effect and then does not allow to quantify any consumption or release of gases in the temperature range lower than 80℃.

However different behaviours are observed for TPS-Raman monitoring of both catalysts. For the bimetallic supported catalyst, from ~80℃ to ~220 ℃, a continuous consumption of $H_2$ is observed whereas the level of $H_2S$ seems to be constant at the cell outlet. Around 220℃, a peak due to $H_2S$ release is clearly observed with an increase of consumption of $H_2$. After this event, both $H_2$ and $H_2S$ concentration profiles slightly increase. At the temperature of $H_2S$ release, while the Co species is almost stable, the $MoS_3$-like phase is transformed into the final $MoS_2$ phase as shown on the concentration profile in Figure 14 (B). Those TPS-Raman results are well in line with those reported in the literature for TPS characterisation of supported molybdenum based catalysts [31] and [32]. On the one hand, the continuous consumption of $H_2$ during the transformation of oxidic molybdenum based species into $MoS_3$ (~80℃-220℃) results from redox reactions involving Mo as suggested by the energy position shift observed for the Mo XANES evolution. On the other hand, the peak release of $H_2S$ is characteristic of $H_2S$ desorption following the reaction pathway $MoS_3 + H_2 \rightarrow MoS_2 + H_2S$ usually proposed for the decomposition of amorphous trisulphide [33]. It is noteworthy that the strong interdependency observed between the Raman gas profile (production/consumption of $H_2S/H_2$ phenomenon) and the concentration profile of the Mo species determined by MCR-ALS gives reliability to the chemometric methods to determine concentration profiles and reveal spectra of pure species.

For the monometallic catalyst, neither consumption nor production of $H_2$ or $H_2S$ is directly detected by TPS-Raman. The quite long sampling of Raman (3 min) required for detecting gases at atmospheric pressure might be responsible for the non-

observation of fast $H_2S$ release for this catalyst. As a matter of fact, the transformation rate of $MoS_3$ into $MoS_2$ for the monometallic supported catalyst appears Figure 14 (A) faster than the one observed for bimetallic supported catalyst Figure 14 (B).

5.4. Characterisation of the final sulphided species

The Mo K edge XAS data of the molybdenum species during the temperature plateau at 400℃ are compared with a bulk $MoS_2$ reference phase on Figure 15Figure *15*. The structural parameters determined by the EXAFS fits are presented in Table 4 (Figure S 7 in supporting information). The final molybdenum phases present in the rising edge a very similar XANES spectrum than the one of the $MoS_2$ phase (Figure 15 (A)) with a well-resolved shoulder around 20017 eV. The slight smoothing of the structures above the main resonance located at 20035 eV compared to the bulk $MoS_2$ phase, and well evidenced in the EXAFS signal, arises from the formation of nanocrystalline $MoS_2$ slabs. In agreement with the literature [31], this is confirmed by the smaller coordination numbers found for the Mo-Mo contribution compared to the one of the $MoS_2$ reference (6 Mo as second neighbours). The identification of the presence of Mo-Co bonds characteristic of the CoMoS phase for the bimetallic sample might be difficult due to the inherent damping of the EXAFS oscillations mainly caused by the high temperature (400℃). Furthermore as the slabs are only partiall y promoted by cobalt, Mo-Co contributions contribute only for a minor extent to the total EXAFS signal at the Mo K edge. The results of the EXAFS fittings of the sulphided $CoMo/Al_2O_3$ catalyst with or without a Mo-Co contribution fixed at the usual distance found in the literature for such a contribution are equivalent as presented on Table 4 (Figure S 7, supporting information).

Table 4: Parameters obtained from the fit of the Mo K edge EXAFS spectra of the sulphided CoMo and Mo catalysts during the plateau of temperature (400℃) ( $\Delta k$ = 3.5-12.5 $Å^{-1}$, $S_0^2$ =0.96, $E_0 + \Delta E$ = 20012.9 eV).

| Backscatterer | N | R (Å) | $\sigma^2$ ($Å^2$) x $10^{-3}$ | R-factor | $\chi^2_\nu$ |
|---|---|---|---|---|---|
| ***Suphided CoMo (400℃)*** | | | | | |
| S | *6* | 2.41 ± 0.01 | 6.7 ± 0.5 | 0.0085 | 269 |
| Mo | 2.6 ± 1.2 | 3.17 ± 0.01 | 7.4 ± 3.0 | | |
| ***Suphided CoMo (400℃)*** | | | | | |
| S | *6* | 2.41 ± 0.01 | | | |
| Mo | 2.5 ± 0.5 | 3.17 ± 0.01 | 6.8 ± 0.5 | 0.0081 | 237 |
| Co | 0.2 ± 0.3 | *2.77* | | | |
| ***Sulphided Mo (400℃)*** | | | | | |
| S | *6* | 2.41 ± 0.01 | 7.2 ± 0.7 | 0.0138 | 2542 |
| Mo | 2.6 ± 1.4 | 3.17 ± 0.01 | 6.2 ± 3.2 | | |

The Co K edge data obtained at the end of the suphidation are presented on Figure 16 with the average of the data measured at 400℃. The $Co_9S_8$ data are presented for comparison purpose. Even if the EXAFS oscillation between the samples and the sulphided reference are in phase, Figure 16 clearly shows that the sulphided species is not only composed of $Co_9S_8$ since the XANES shape and the distance of the first coordination shell are different (Co-S contribution at 2.41 Å for the catalysts compared to a distribution of distances 2.09-2.24 Å for the $Co_9S_8$ reference). As presented in Table 5 (Figure S 8, supporting information), it is noteworthy that the best EXAFS fitting for the bimetallic sample is obtained with a Co-Mo contribution (0.9 (1.0) Mo at 2.76 (0.06) Å) characteristic of the CoMoS phase [31]. Then at the opposite of the fitting carried out at the Mo Kedge for the final sulphided sample, the EXAFS analysis of the bimetallic catalyst carried out at the Co K edge leads to the conclusive formation of the CoMoS species. This finding supports very well the conclusion of the simultaneous monitoring of sulphidation of Co and Mo centers for the bimetallic catalyst discussed in the previous section.

Table 5: Parameters obtained from the fit of the Co K edge EXAFS spectra of the sulphided $CoMo/Al_2O_3$ catalyst during the plateau of temperature (400℃) ($\Delta k$ = 2.9-9.5 $Å^{-1}$, $S_0^2$ =0.48, $E_0 + \Delta E$ = 7719.6 eV).

| **Backscatterer** | **N** | **R (Å)** | **$\sigma^2$ (Å²) x $10^{-3}$** | **R-factor** | **$\chi^2_\nu$** |
|---|---|---|---|---|---|
| ***Sulphided dried CoMo (400℃)*** | | | | | |
| S | 5.2 ± 1.2 | 2.22 ± 0.01 | 5.8 ± 3.2 | 0.01074 | 100 |
| Mo | 0.9 ± 1.0 | 2.76 ± 0.06 | | | |

## 6. Conclusion

In this paper we demonstrated that the characterisation of heterogeneous catalysts by XAS spectroscopy at the SOLEIL's Quick-EXAFS beamline has reached a quite mature level from an experimental and analytical point of view.

Firstly, we demonstrated how powerful are the chemometric tools, such as PCA and MCR-ALS methods for solving the speciation of evolving catalysts under realistic conditions. The determination of pure spectra of intermediate species deduced from MCR-ALS analysis is of prime importance for the chemical identification of the species involved in the process and then for a full understanding of the transformations suffered by the catalysts during reaction. Additionally, the access to the pure spectra can be sometimes unique if the spectra of intermediate species do not exist in any library of XAS spectra. In the case of catalysis, in which species are well dispersed at the surface of a support, the transformation of these species leads to something unique, often different from the known bulk phases for which spectra are reported in the literature [8d]. Nevertheless, despite the power of such chemometric methods, results so-obtained must be critically analysed. The local order structure which can be extracted from the analysis of the EXAFS data of the MCR-ALS components must be related to meaning-full structures reported in the literature in order to avoid the discovery of a sheep with five legs or at least ascertained by complementary information coming for instance from Raman spectroscopy of the sample. Herein the

simultaneous monitoring of sulphidation by TPS-Raman gives complementary information emphasizing how reliable is the time-resolved speciation of Mo species determined by MCR-ALS for the bimetallic supported catalyst.

Secondly, thanks to the good time-resolution provided by the Quick-EXAFS monochromators and catalytic cell available at the SOLEIL's Quick-XAS beamline, the speciation of Mo-based phases for the two supported Mo catalysts over alumina has been analysed in depth upon activation. It has been shown that the introduction of the cobalt promoter changes the molybdenum sulphidation pathway, accelerating the formation of fully sulphided phase everything else being equal. Namely, a 3-stepped route has been evidenced for the bimetallic CoMo supported catalyst involving the transformation of the oxidic precursor into an assumed $MoS_3$-like phase and then $MoS_2$ phase. The sulphidation of the monometallic Mo-based catalyst involved a 4-stepped mechanism, with first the transformation of the oxidic precursors into an oxysulphide species, then a $MoS_3$-like phase and finally the final $MoS_2$ phase. It is noteworthy that the lack of complementary information on the chemical nature of sulphur ligands forming the oxysulphide species does not allow us to propose a model for this intermediate. Such limitation will be overcome with a future work in which the complementary use of Raman and Quick-XAS spectroscopies, both used for the catalyst characterisation, will allow to give us more insight about the formation of such oxysulphide species [34]. Using the edge jumping capability of the SOLEIL's quick-EXAFS monochromators, it was also pointed out, comparing the concentration profiles of Co- and Mo-based species, that about 40% of metals are concomitantly sulphided providing good conditions to form the CoMoS active species. As a matter of fact the formation of the CoMoS active species is confirmed by the Co K edge fitting of the final sulphide species with the presence of a Co-Mo contribution fitted at 2.76 Å.

Acknowledgement

The authors are grateful to SOLEIL committees for beam time allocated on the SAMBA beamline. Elodie Devers and Antoine Hugon are grateful for fruitful discussions.

† Supporting information for this article is available on the web under http://www.xxxxx or from the author.

## 7. References

[1] (a) A. Rochet, V. Moizan, V. Briois, C. Pichon, Diamond Light Source Proceedings, 1 (2010), e130; (b) E. Payen, L. Barthe, E. Berrier, J. Blanchard, V. Briois, X. Carrier, M. Che, S. Cristol, A. Griboval-Constant, J. Hong, Y. Joly, A. Khodakov, C. La Fontaine, E. Marceau, P. Massiani, A. Tougerti, Actual. Chim. 356 (2011) 20; (c) C. La Fontaine, L. Barthe, A. Rochet, V. Briois, Catal. Today 205 (2013) 148.

[2] E. Fonda, A. Rochet, M. Ribbens, L. Barthe, S. Belin, V. Briois, J. Synch. Radiat. 19 (2012) 417.

[3] S. Belin, V. Briois, A. Traverse, M. Idir, T. Moreno, M. Ribbens, Physica Scripta T115 (2005) 980.

[4] C. S. Song, Catal. Today 86 (2003) 11.

[5] H. Topsøe, R. Candia, N.-Y. Topsøe, B. S. Clausen, Bull. Soc. Chim. Belg. 93 (1984) 783.

[6] B. Ravel, M. Newville, J. Synch. Radiat. 12 (2005) 537.

[7] M. Newville, J. Synch. Radiat. 8 (2001) 322.

[8] (a) R. M. Wang, O. Dmitrieva, M. Farle, G. Dumpich, H. Q. Ye, H. Poppa, R. Kilaas, C. Kisielowski, Phys. Rev. Lett. 100 (2008) 017205; (b) K. M. McPeak, M. A. Becker, N. G. Britton, H. Majidi, B. A. Bunker, J. B. Baxter, Chem. Mater. 22 (2010) 6162; (c) H. W. P. Carvalho, S. H. Pulcinelli, C. V. Santilli, F. Leroux, F. Meneau, V. Briois, Chem. Mater. 25 (2013) 2855; (d) W. H. Cassinelli, L. Martins, A. R. Passos, S. H. Pulcinelli, C. V. Santilli, A. Rochet, V. Briois, Catal. Today 229 (2014) 114.

[9] A. Manceau, M. Marcus, T. Lenoir, J. Synch. Radiat. 21 (2014) 1140.

[10] (a) P. Conti, S. Zamponi, M. Giorgetti, M. Berrettoni, W. H. Smyrl, Anal. Chem. 82 (2010) 3629; (b) A. Voronov, A. Urakawa, W. v. Beek, N. E. Tsakoumis, H. Emerich, M. Rønning, Anal. Chim. Acta 840 (2014) 20.

[11] (a) C. A. Nunes, E. C. Resjende, I. R. Guimaraes, A. S. Anastacio, M. C. Guerreiro, Appl. Spectrosc. 65 (2011) 692; (b) M. Staniuk, O. Hirsch, N. Kränzlin, R. Böhlen, W. van Beek, P. M. Abdala, D. Koziej, Chem. Mater. 26 (2014) 2086; (c) J. Hong, E. Marceau, A. Y. Khodakov, L. Gaberová, A. Griboval-Constant, J.-S. Girardon, C. La Fontaine, V. Briois, ACS Catalysis 5 (2015) 1273.

[12] (a) S. R. Wasserman, J. Phys. IV. 7 (1997) 203; (b) S. R. Wasserman, P. G. Allen, D. K. Shuh, J. J. Bucher, N. M. Edelstein, J. Synch. Radiat. 6 (1999) 284.

[13] A. C. Faro Jr, V. O. Rodrigues, J.-G. Eon, A. S. Rocha, Quimica Nova 33 (2010) 1342.

[14] J. Jaumot, R. Gargallo, A. de Juan, R. Tauler, Chemom. Intell. Lab. Syst. 76 (2005) 101.

[15] H. Ohtsuka, T. Tabata, O. Okada, L. M. F. Sabatino, G. Bellussi, Catal. Letters 44 (1997) 265.

[16] B. Jongsomjit, J. Panpranot, J. G. Goodwin Jr, J. Catal. 204 (2001) 98.

[17] E. Payen, J. Grimblot, S. Kasztelan, J. Phys. Chem 91 (1987) 6642.

[18] L. Le Bihan, P. Blanchard, M. Fournier, J. Grimblot, E. Payen, J. Chem. Soc. Faraday Trans. 94 (1998) 937.

[19] (a) C. Lamonier, D. Soogund, J. Mazurelle, P. Blanchard, D. Guillaume, E. Payen, Origin of the dispersion limit in the preparation of Ni(Co) $Mo/Al_2O_3$ and Ni(Co)$Mo/TiO_2$ HDS oxidic precursors, Vol.162, 2006, p.713; (b) J. Moreau, O. Delpoux, E. Devers, M. Digne, S. Loridant, Langmuir 29 (2013) 207.

[20] A. M. Beale, G. Sankar, Chem. Mater. 15 (2002) 146

[21] A. Tougerti, E. Berrier, A.-S. Mamede, C. La Fontaine, V. Briois, Y. Joly, E. Payen, J.-F. Paul, S. Cristol, Angew. Chem. Int. Ed. 125 (2013) 6568.

[22] A. Rochet, B. Baubet, V. Moizan, E. Devers, A. Hugon, C. Pichon, E. Payen, V. Briois, submitted to J. Phys Chem C.

[23] D. Nicosia, R. Prins, J. Catal. 231 (2005) 259.

[24] R. Cattaneo, F. Rota, R. Prins, J. Catal.199 (2001) 318.

[25] P. Afanasiev, H. Hobic, C. Lorentz, P. Leverd, N. Mastubayashi, L. Piccolo, M. Vrinat, J. Phys. Chem. C 113 (2009) 4139.

[26] P. Afanasiev, I. Bezverkhy, Chem. Mater. 14 (2002) 2826.

[27] S. Reschke, K. G. V. Sigfridsson, P. Kaufmann, N. Leidel, S. Horn, K. Gast, C. Schulzke, M. Haumann, S. Leimkühler, J. Biol. Chem. 288 (2013) 29736.

[28] K. G. V. Havelius, S. Reschke, S. Horn, A. Döring, D. Niks, R. Hille, C. Schulzke, S. Leimkühler, M. Haumann, Inorg. Chem. 50 (2011) 741.

[29] (a) T. Weber, J. C. Muijsers, J. W. Niemantsverdriet, J. Phys. Chem 99 (1995) 9194; (b) S. P. Cramer, K. S. Liang, A. J. Jacobson, C. H. Chang, R. R. Chianelli, Inorg. Chem. 23 (1984) 1215.

[30] (a) W. Clegg, N. Mohan, A. Mueller, A. Neumann, W. Rittner, G. M. Sheldrick, Inorg. Chem.19 (1980) 2066; (b) D. Genuit, I. Bezverkhyy, P. Afanasiev, J. Solid State Chem. 178 (2005) 2759; (c) J.-H. Chou, J. A. Hanko, M. G. Kanatzidis, Inorg. Chem. 36 (1997) 4.

[31] L R. G. Leliveld, A. J. van Dillen, J. W. Geus, D. C. Koningsberger, J. Catal. 165 (1997) 184.

[32] P. Arnoldy, P., J. A. M. van den Heijkant, G. D. de Bok, J. A. Moulijn, J. Catal. 92 (1985) 35.

[33] (a) J. L. Brito, M. Ilija, P. Hernández, Thermochimica Acta 256 (1995) 325; (b) J. Whelan, I. Banu, G. E. Luckachan, N. D. Banu, S. Stephen, A. Tharalekshmy, S. Al Hashimi, R. V. Vladea, M. S. Katsiotis, S. M. Alhassan, JAST 6 (2015) 1.

[34] A. Rochet, B. Baubet, V. Moizan, E. Devers, A. Hugon, C. Pichon, E. Payen, V. Briois, in preparation.

Figure captions

Figure 1: Picture of the *in situ* cell with a Raman gas probe installed at the cell outlet.

Figure 2: XAS data acquisition sequence switching between Mo and Co K edges with simultaneous Raman gas analysis. The colored arrows mark the time required for edge jump (changing the monochromator, reference metallic foil, amplifier gains and gases filling the ICs).

Figure 3: Schematic representation of the multivariate curve resolution analysis of the time-resolved experimental XAS data *D.* In the MCR-ALS method *C* and $S^T$ are the concentration matrix of the pure species and the pure XAS spectra matrix, respectively. In the PCA analysis, *C* is the column matrix corresponding to the weight of each principal component described in the row matrix $S^T$.

Figure 4: Plot of the first six PCA components obtained during the study of the sulphidation process of the bimetallic dried $CoMo/Al_2O_3$ catalyst. Each component is weighted by its respective eigenvalue: 522.802 for PCA1, 9.105 or PCA2, 1.477 for PCA3, 0.533 for PCA4, 0.279 for PCA5 and 0.210 for PCA6.

Figure 5: Scree plot of the eigenvalues obtained by PCA of the Mo K edge data for the bimetallic CoMo (A) and monometallic Mo (B) supported catalysts. The eigenvalues are presented with a linear scale (right scale) for the PCA performed on the derivatives spectra (line) and with a log scale (left scale) for the XAS data (symbol). Corresponding cumulative explained variances considering increasing number of components are specified for the first components obtained with the PCA on derivatives. The grey lines are used as guide for eyes for the results obtained with the XAS spectra.

Figure 6: Raman spectra of the oxidic monometallic $Mo/Al_2O_3$ (A) and bimetallic $CoMo/Al_2O_3$ (B) catalysts at different Regions Of Interest.

Figure 7: Mo K edge XANES (A), EXAFS spectra (B) and corresponding Fourier transform moduli (C) at RT for the oxidic bimetallic CoMo (black) and monometallic Mo (red) supported catalysts compared to reference samples.

Figure 8: Linear combination fittings of the Mo K edge EXAFS spectra recorded for the oxidic bimetallic CoMo (A) and monometallic Mo (B) supported catalysts.

Figure 9: Co K edge XANES (A), EXAFS spectra (B) and corresponding Fourier transform moduli (C) at RT for the oxidic bimetallic CoMo supported catalyst compared to reference samples. The EXAFS and FT signals of the $Co_3O_4$ reference are presented with a factor of 0.5 for sake of clarity.

Figure 10: *In situ* monitoring of the sulphidation by Quick-XAS at the Mo K edge for the monometallic $Mo/Al_2O_3$ catalyst (A) and at the Mo K edge (B) and Co K edge (C) for the bimetallic $CoMo/Al_2O_3$ catalyst.

Figure 11: *In situ* monitoring of the sulphidation by Quick-XAS at the Mo K edge for the bimetallic $CoMo/Al_2O_3$ catalyst (top) and the monometallic $Mo/Al_2O_3$ catalyst (bottom): Fourier transform moduli.

Figure 12: Mo K edge XANES (A), EXAFS spectra (B) and corresponding Fourier transform moduli (C) of the intermediate species determined by MCR-ALS for the bimetallic CoMo supported catalyst.

Figure 13: Mo K edge XANES (A), EXAFS spectra (B) and corresponding Fourier transform moduli (C) of the intermediate species determined by MCR-ALS for the monometallic Mo supported catalyst.

Figure 14: Top: Concentration profile of components determined by MCR-ALS as a function of the temperature during sulphidation of the monometallic Mo (A) and bimetallic CoMo (B) supported catalysts. Bottom: Corresponding Raman gas profiles of $H_2$ and $H_2S$ signals obtained during the sulphidation process of both catalysts.

Figure 15: Mo K edge XANES (A), EXAFS spectra (B) and corresponding Fourier transform moduli (C) obtained during the plateau of temperature (400℃) of the monometallic and bimetallic catalysts. The $MoS_2$ reference data (RT) are presented for comparison purpose. The EXAFS and FT signals of the $MoS_2$ reference are presented with a factor of 0.5 for sake of clarity.

Figure 16: Co K edge XANES (A), EXAFS spectra (B) and corresponding Fourier transform moduli (C) obtained during the plateau of temperature (400℃) of the bimetallic catalysts. The data of $Co_9S_8$ (RT) are presented for comparison purpose.

**Figure 1**

Click here to download high resolution image

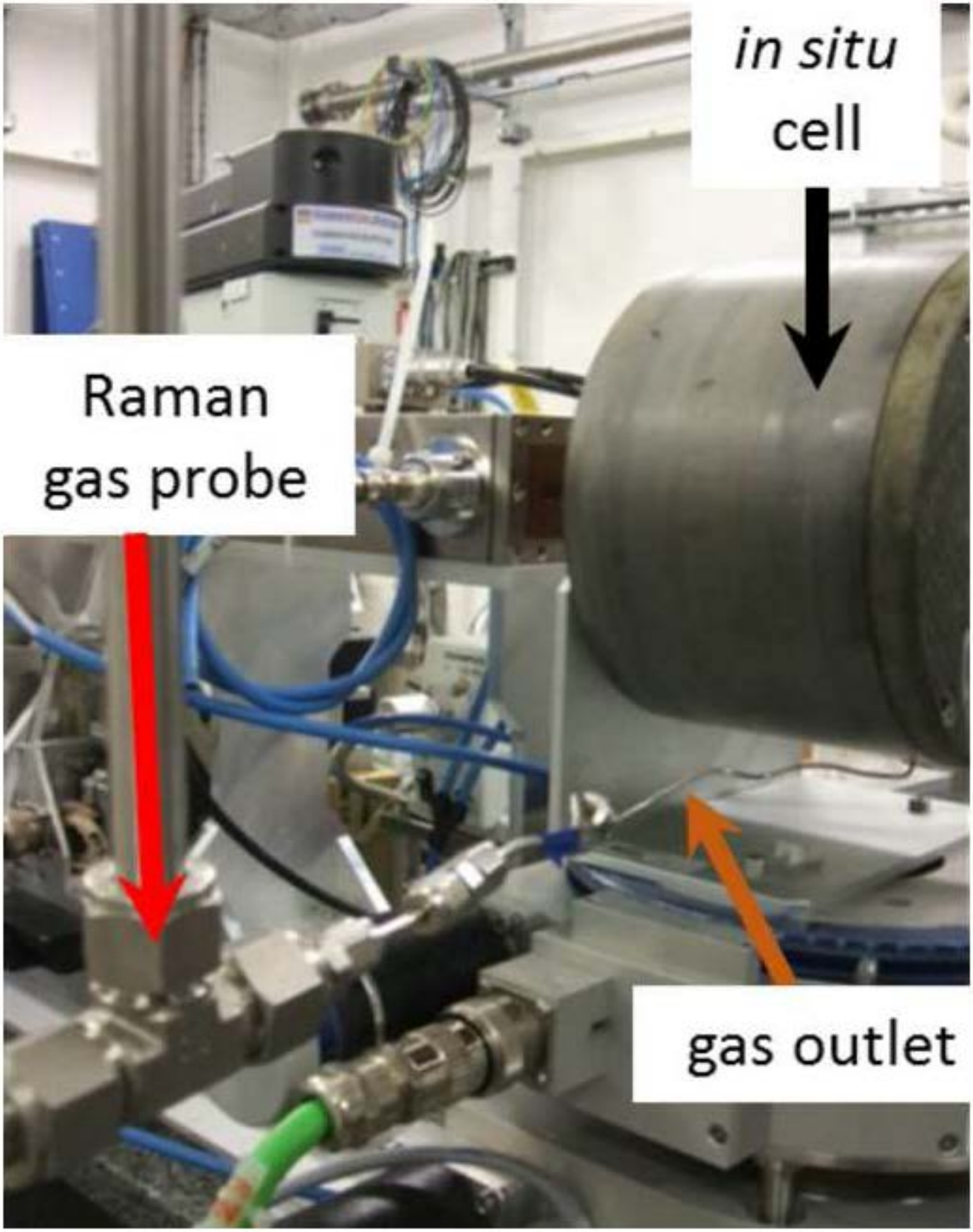

Figure 2

Click here to download high resolution image

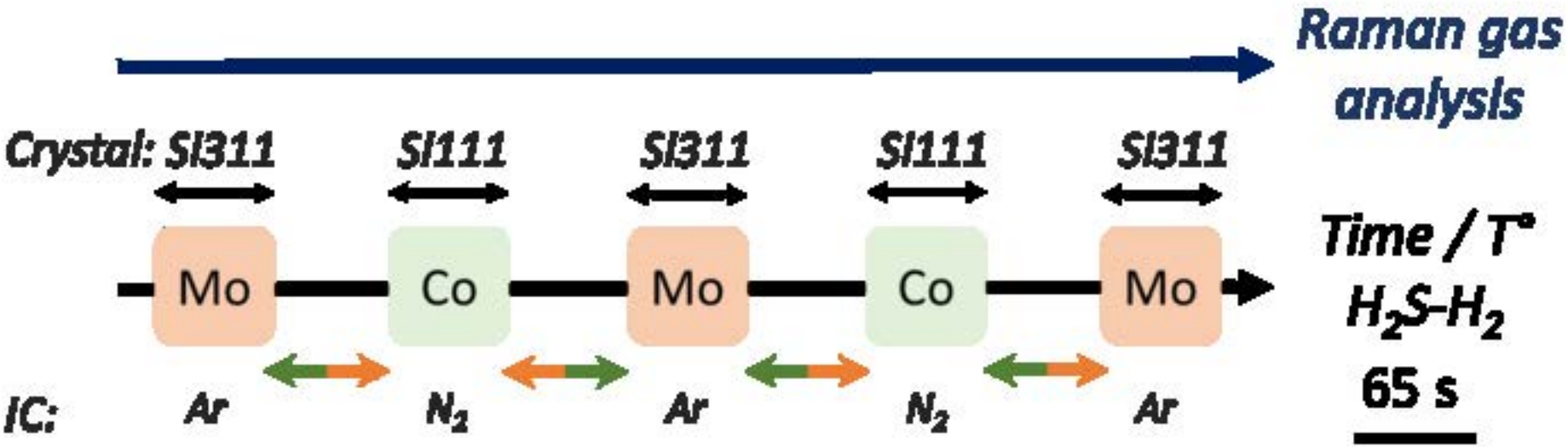

Figure 3

Click here to download high resolution image

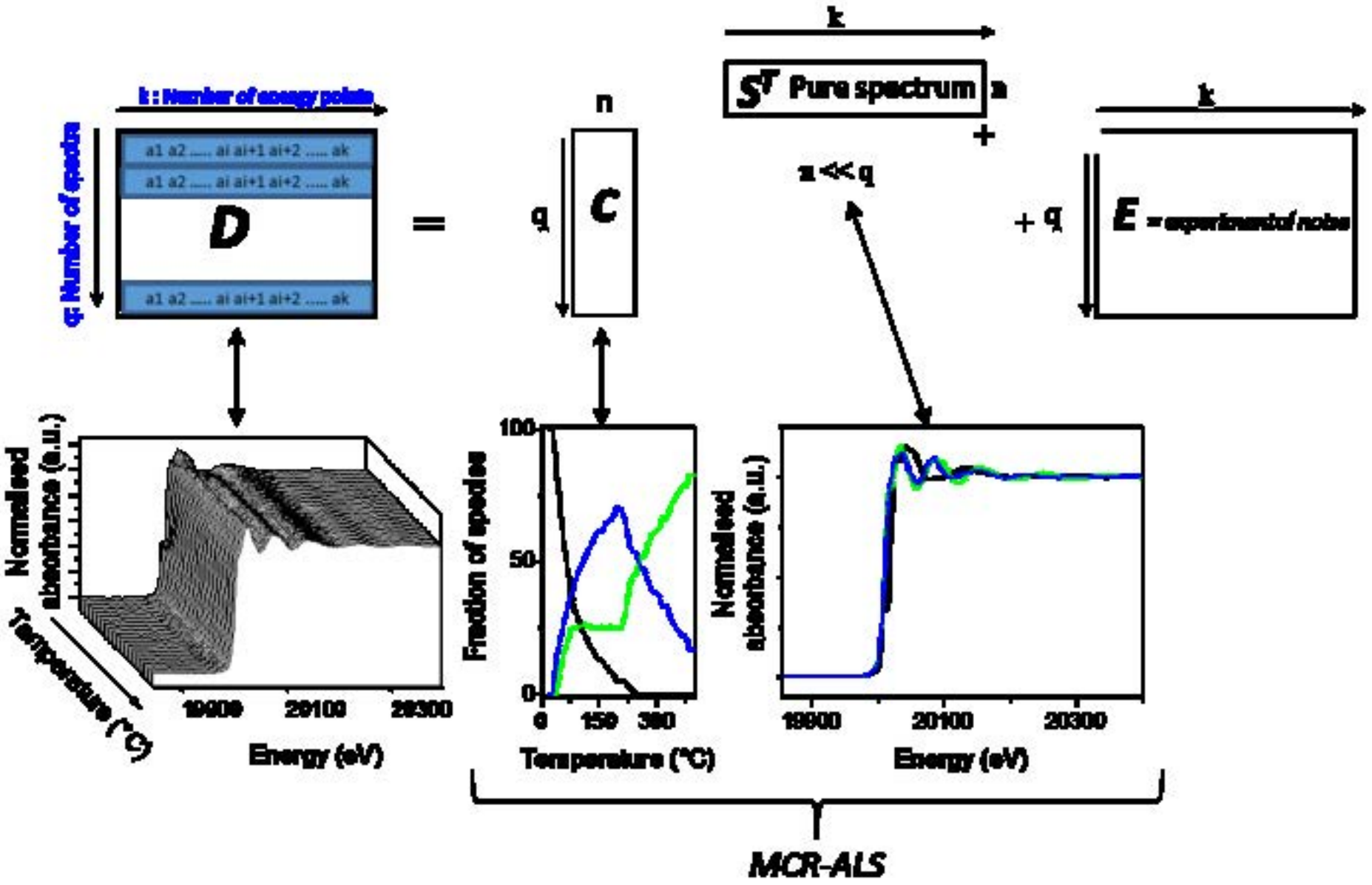

Figure 4

Click here to download high resolution image

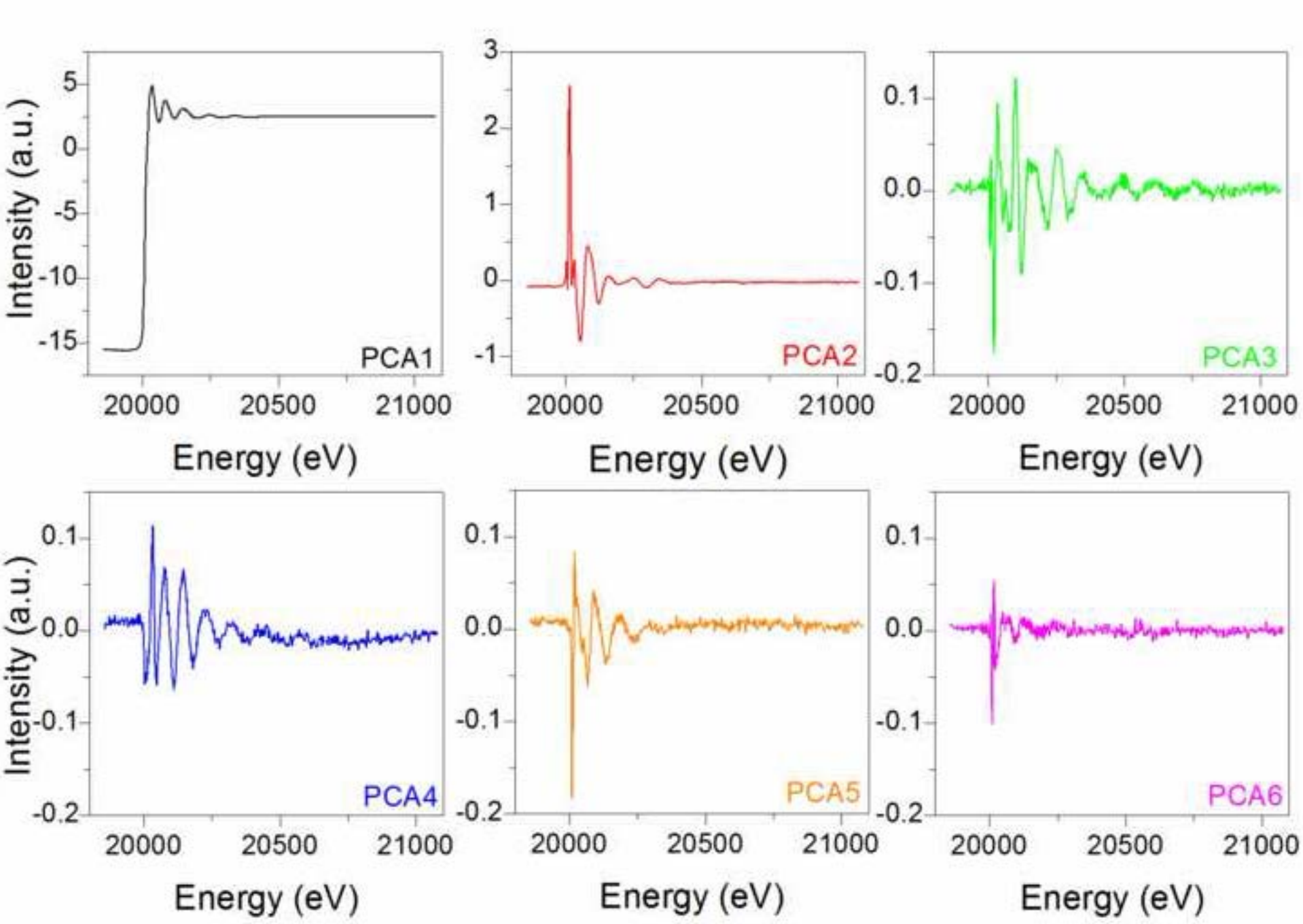

Figure 5A

Click here to download high resolution image

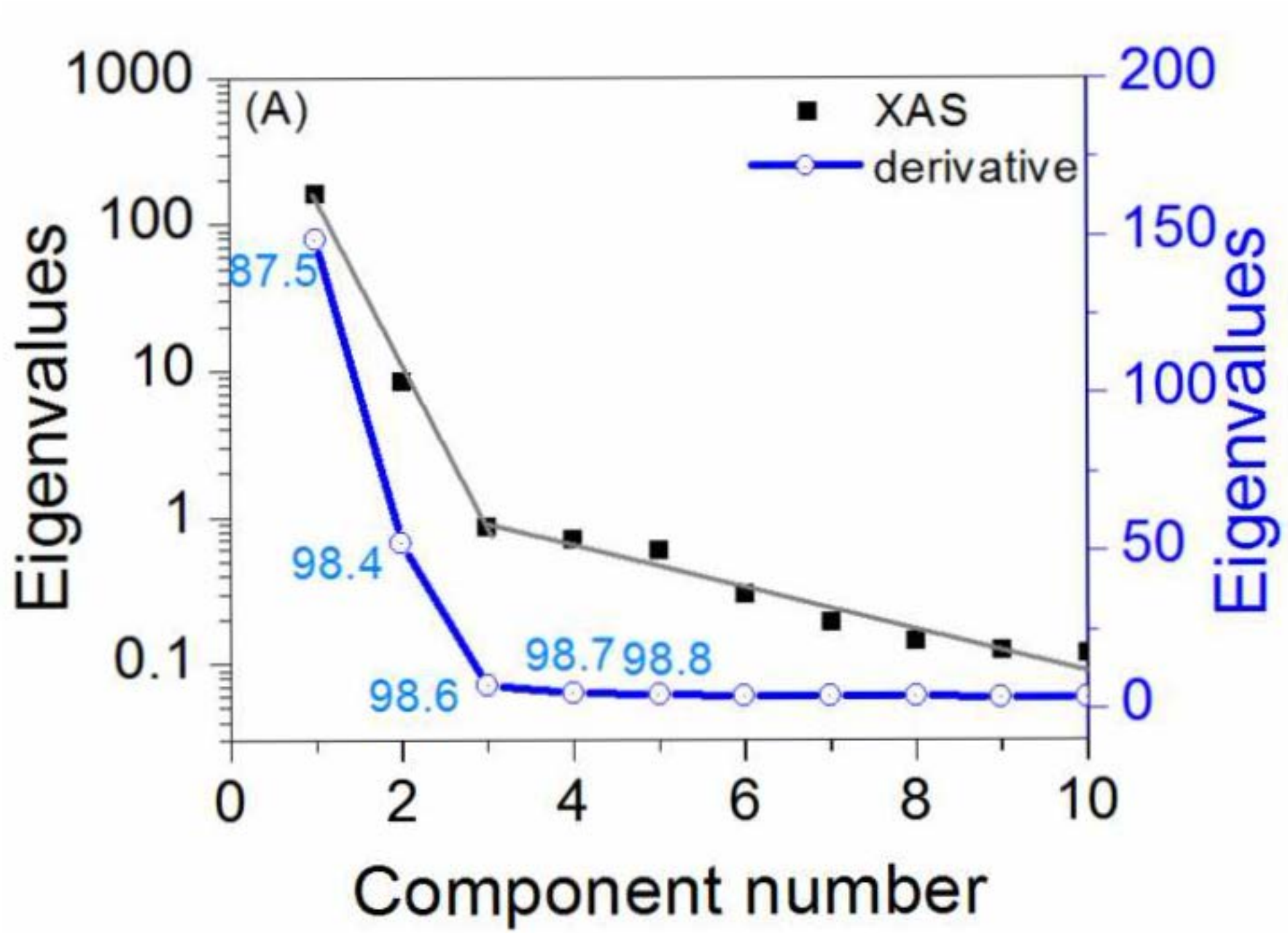

Figure 5B

Click here to download high resolution image

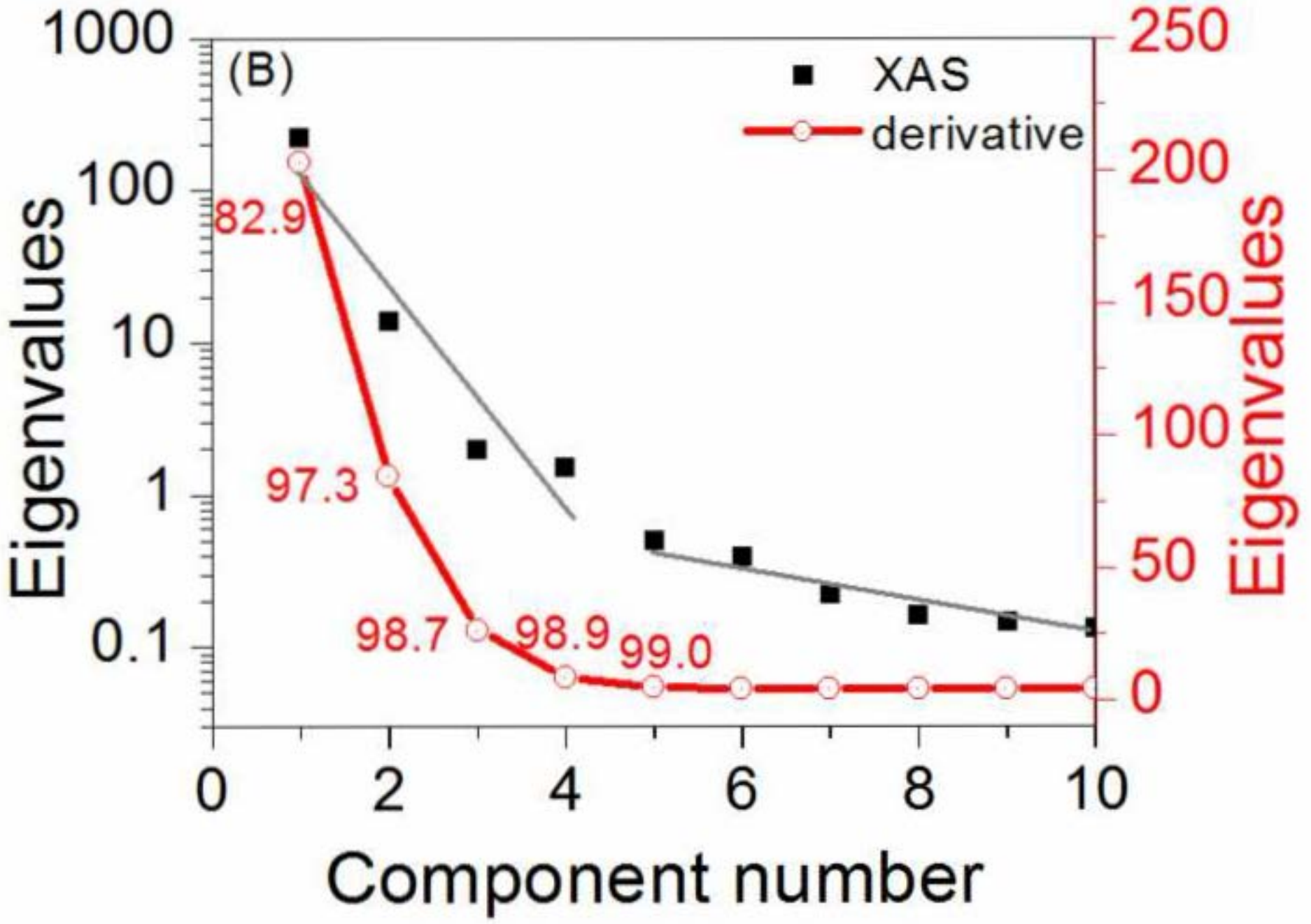

**Figure 6**

Click here to download high resolution image

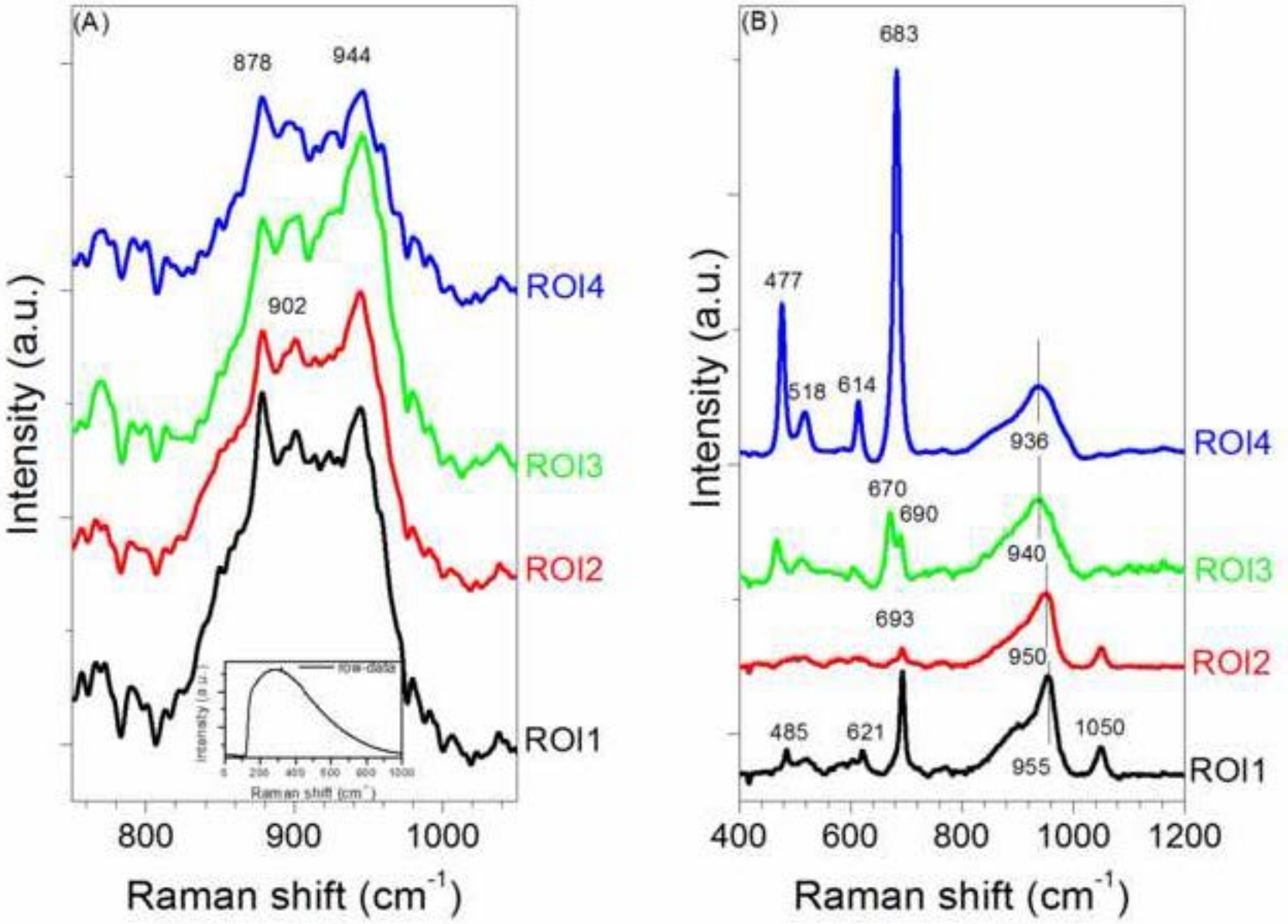

**Figure 7**

Click here to download high resolution image

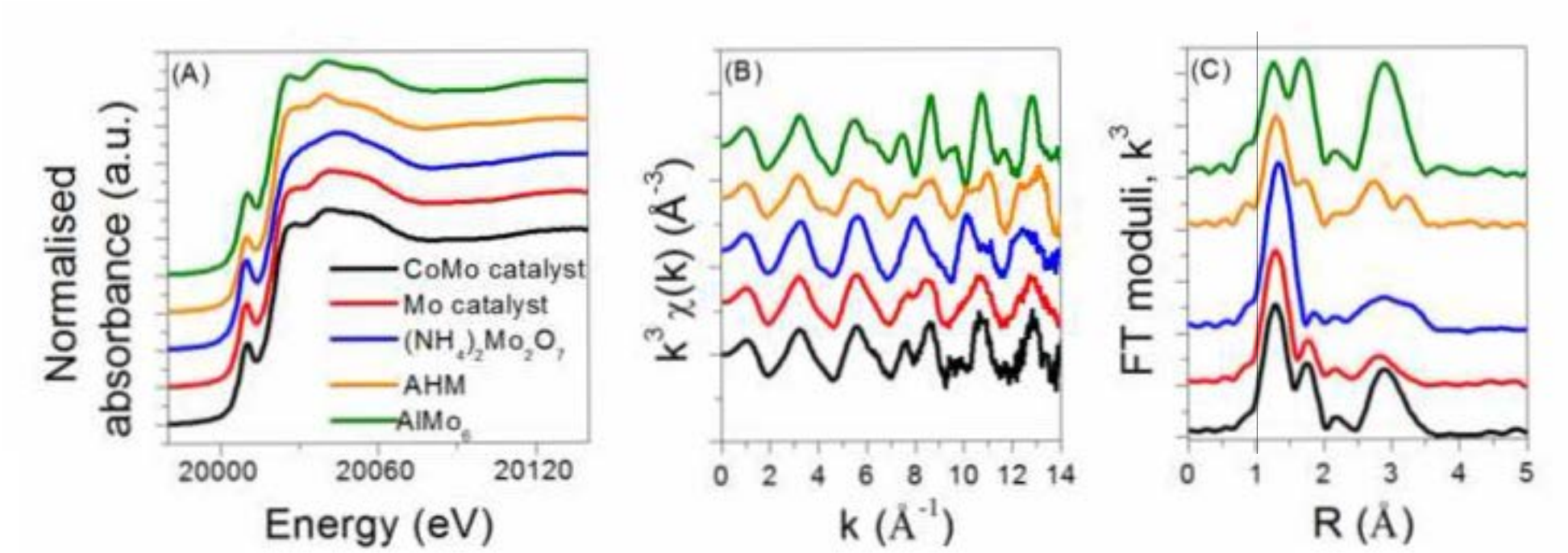

**Figure 8**

Click here to download high resolution image

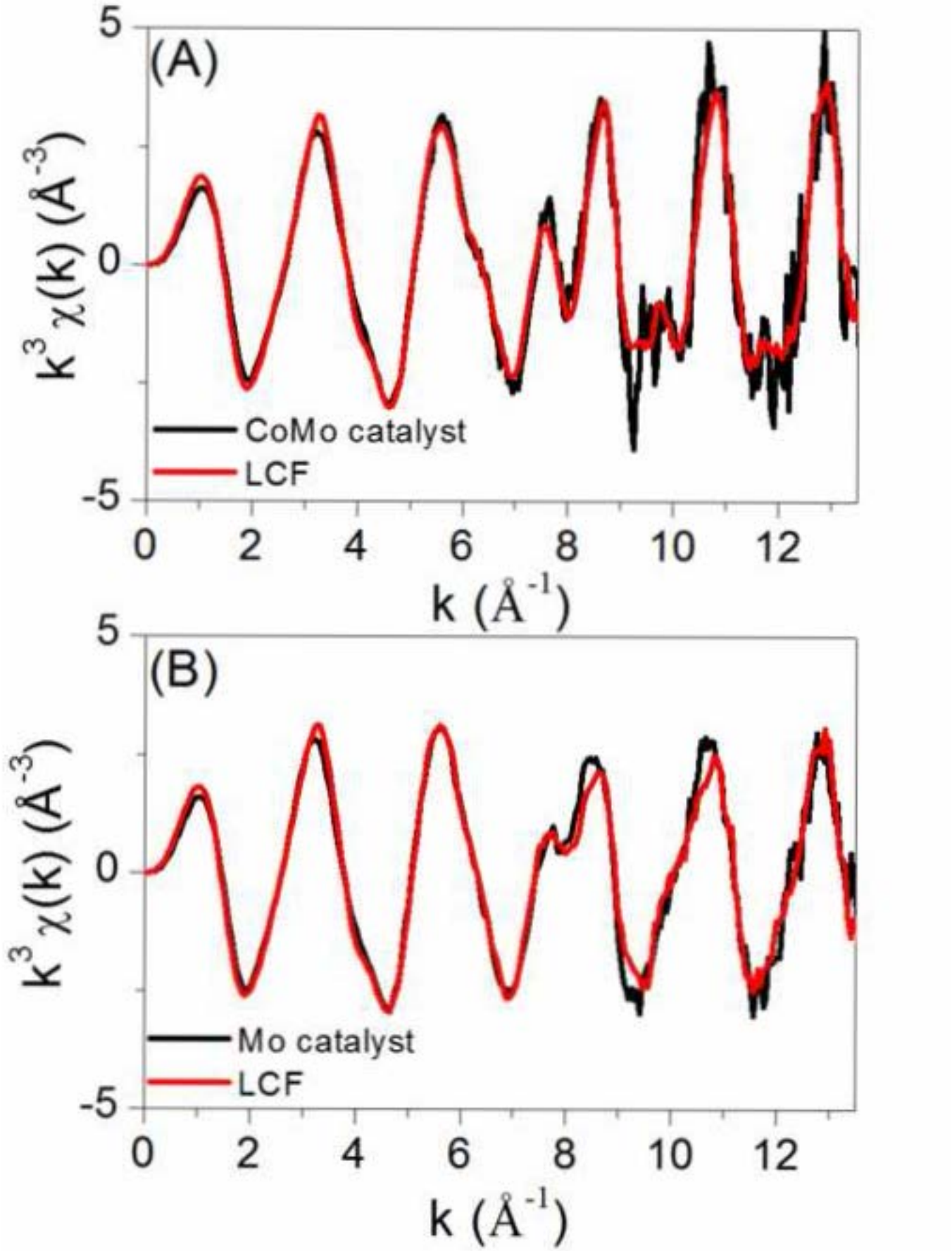

**Figure 9**

**Click here to download high resolution image**

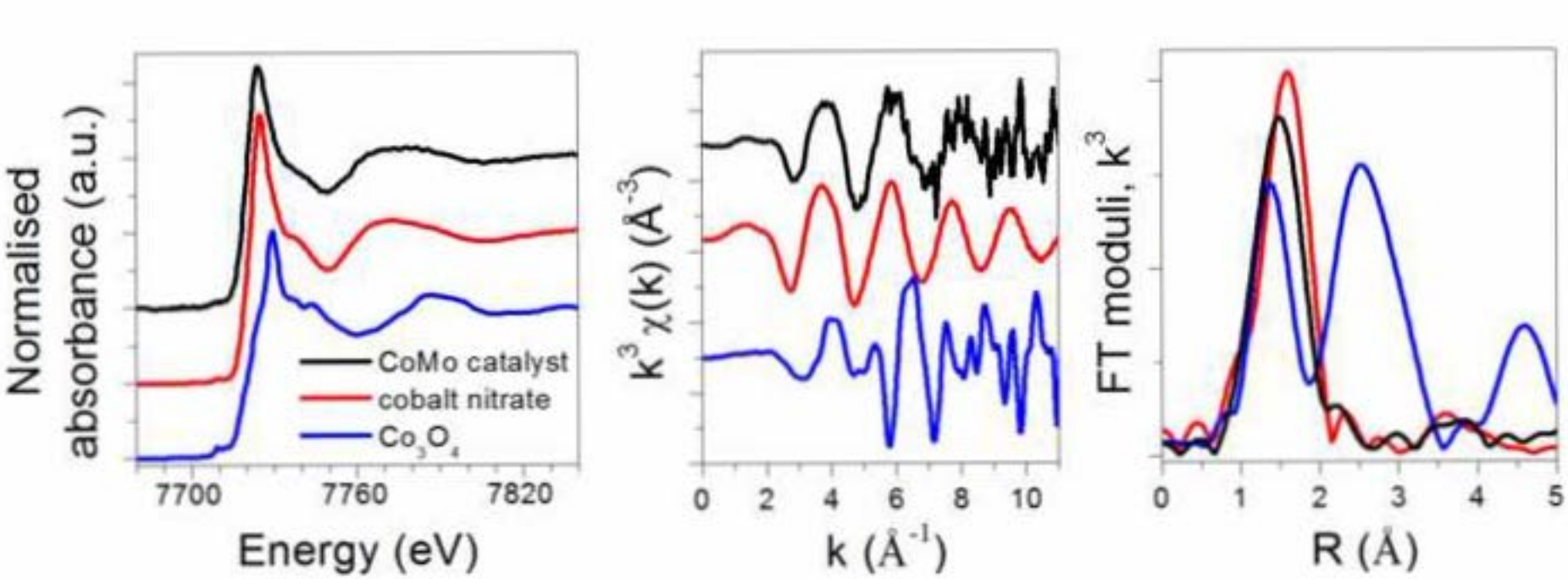

**Figure 10A**

Click here to download high resolution image

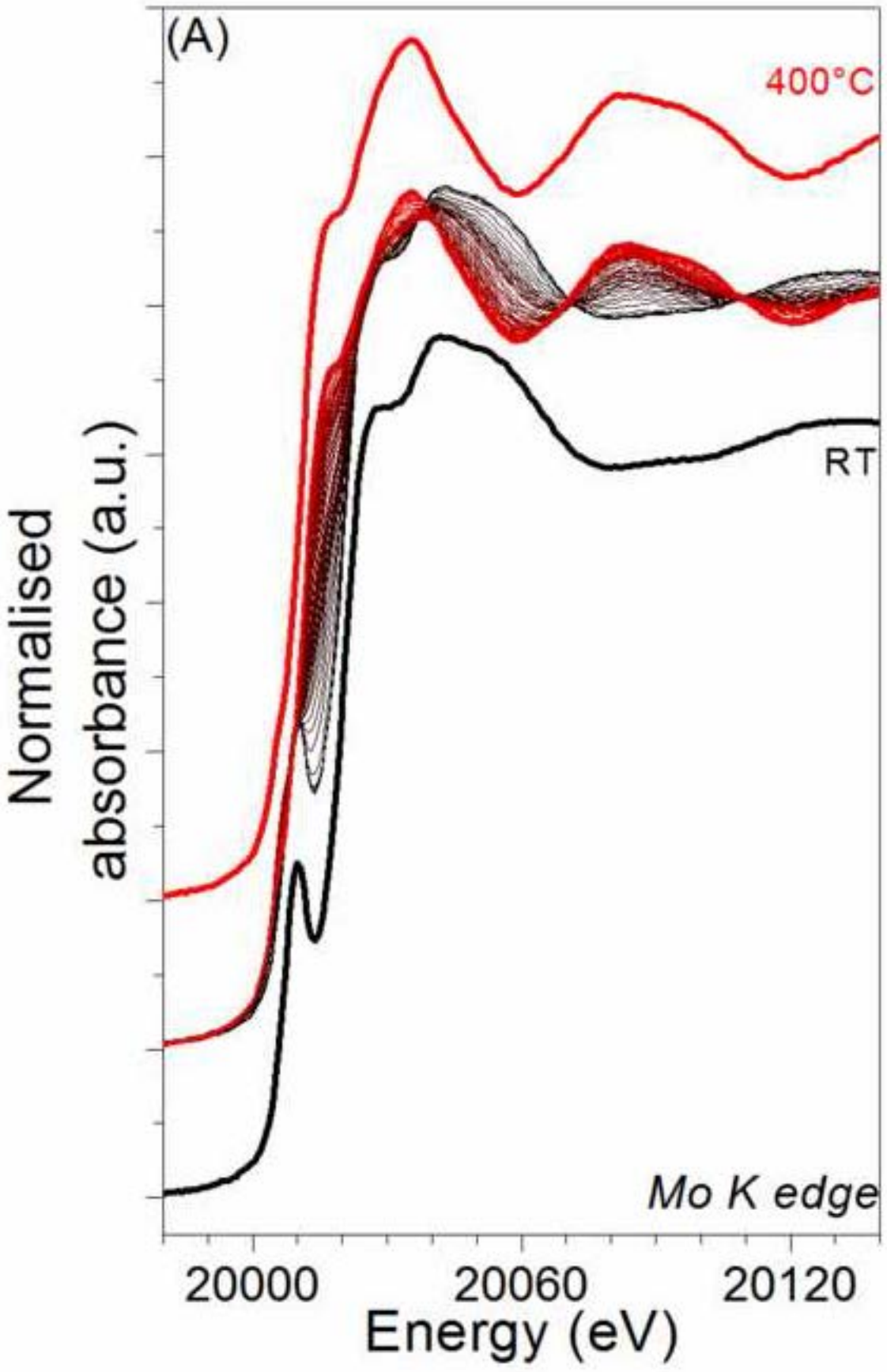

Figure 10B-C

Click here to download high resolution image

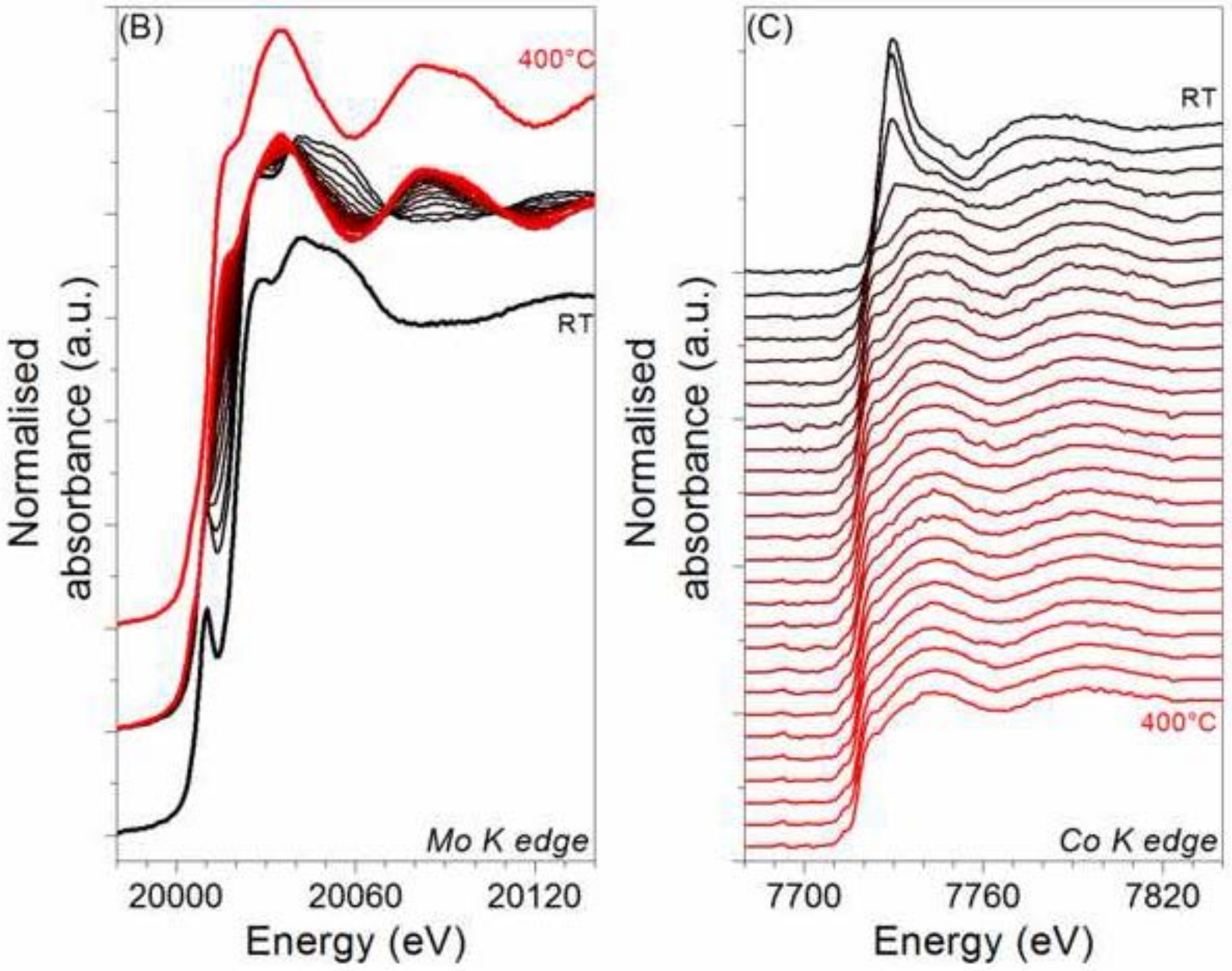

**Figure 11-TOP**

**Click here to download high resolution image**

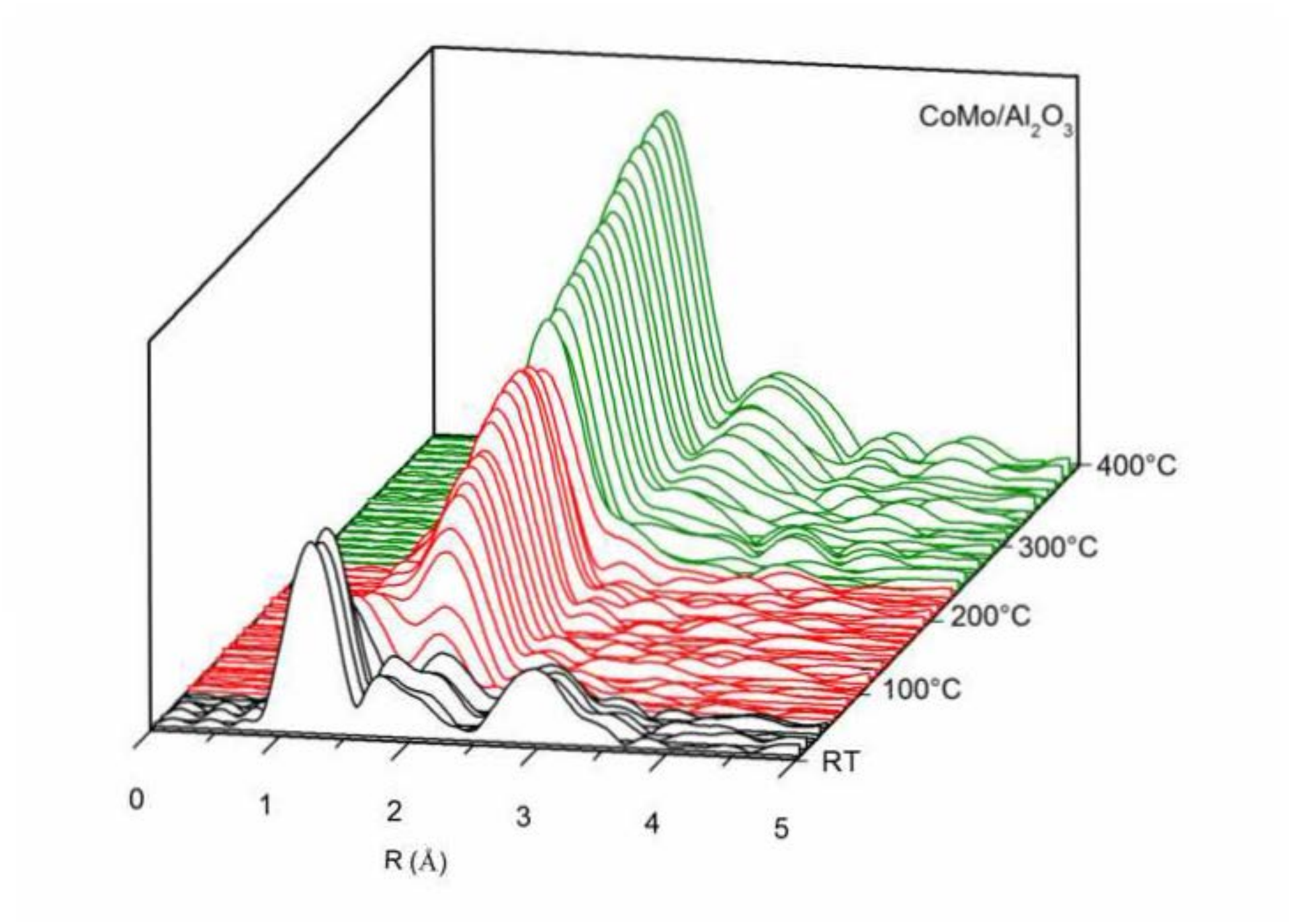

**Figure 11-BOTTOM**

**Click here to download high resolution image**

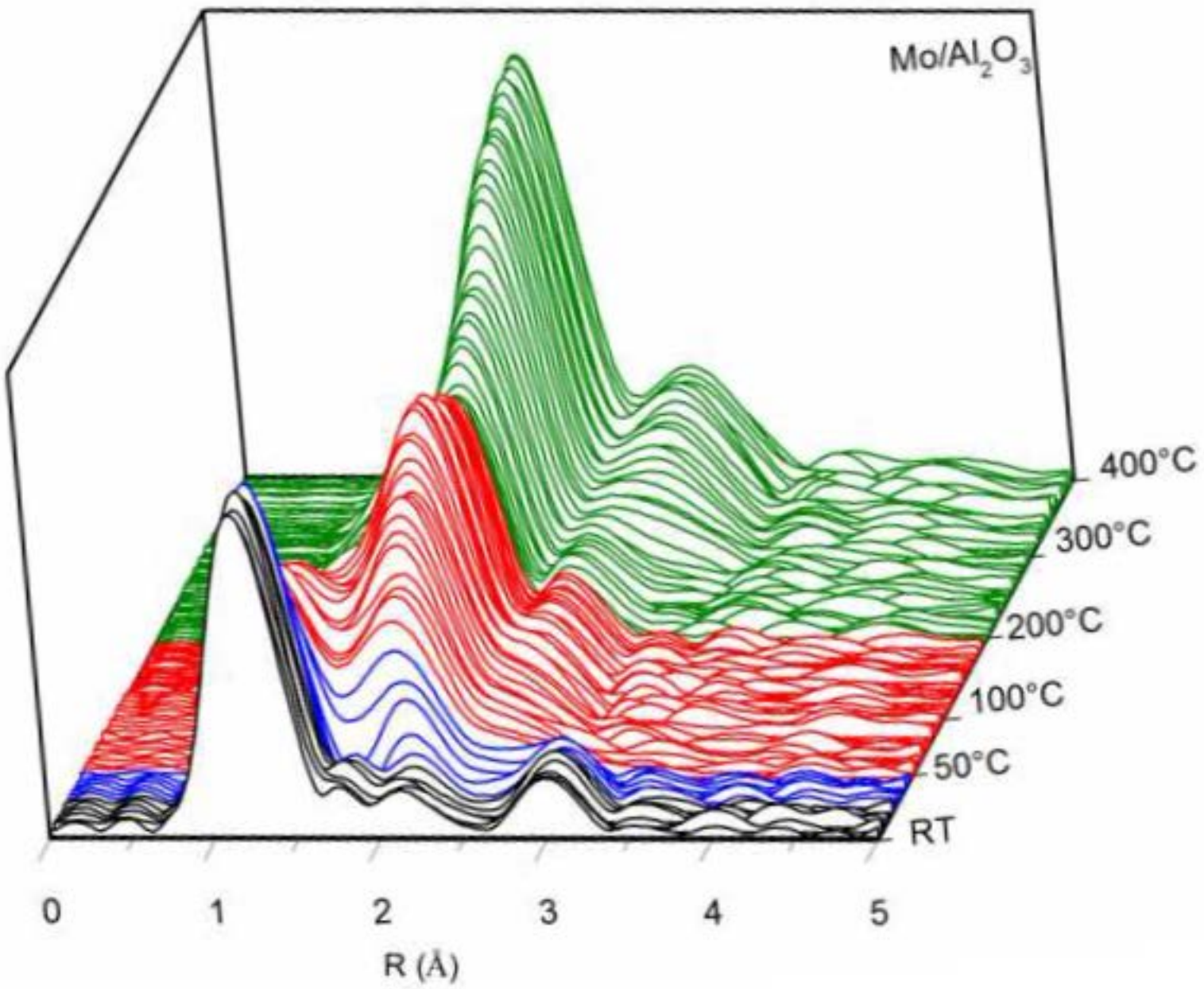

**Figure 12**

Click here to download high resolution image

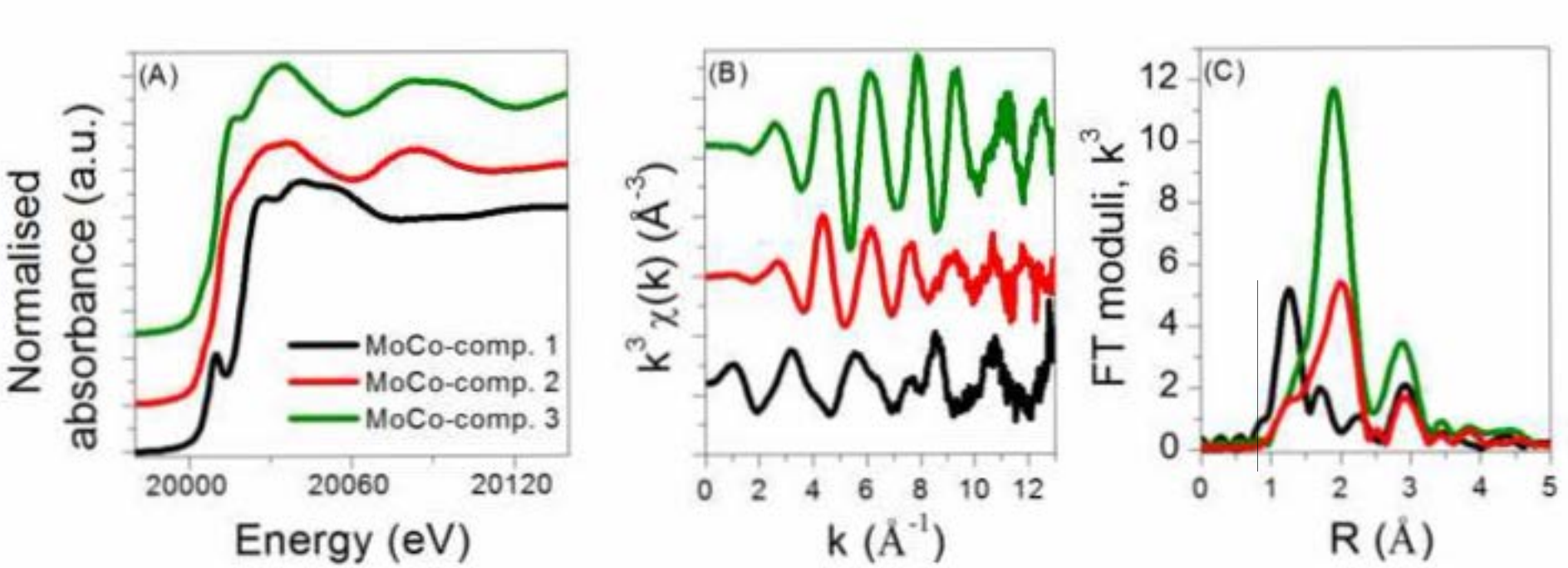

**Figure 13**

Click here to download high resolution image

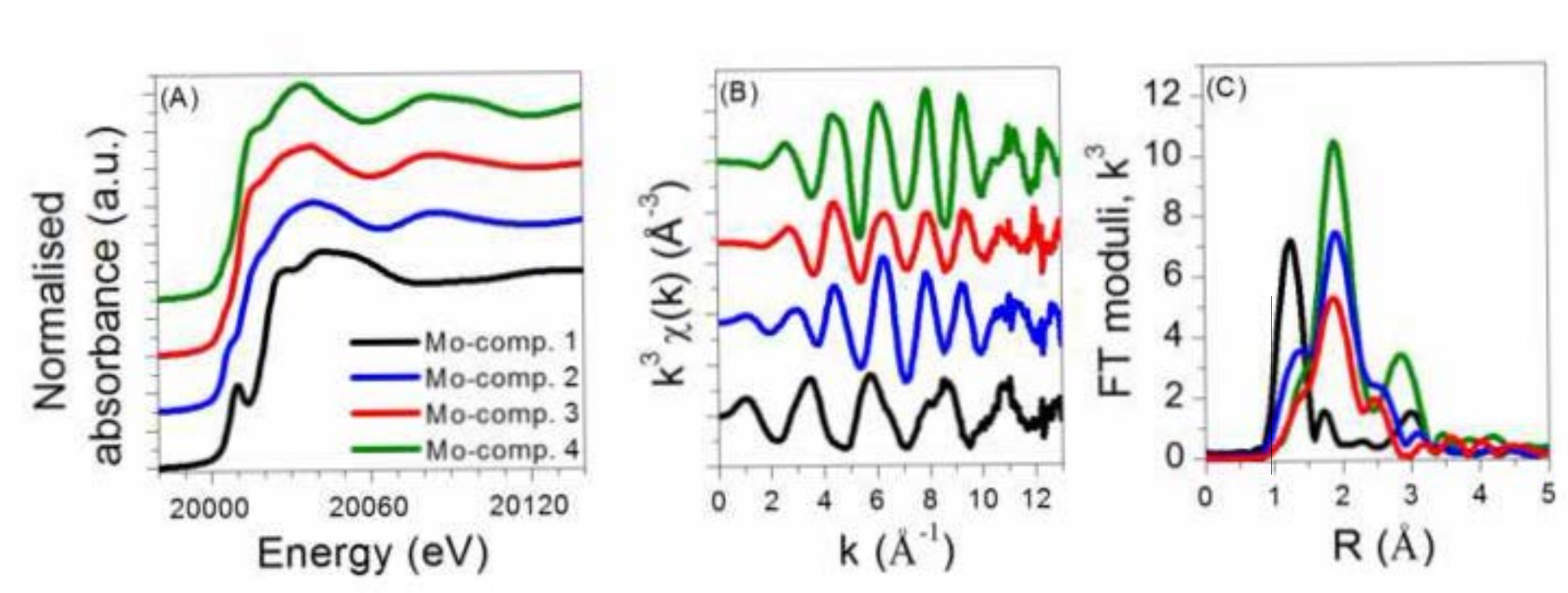

**Figure 14**

Click here to download high resolution image

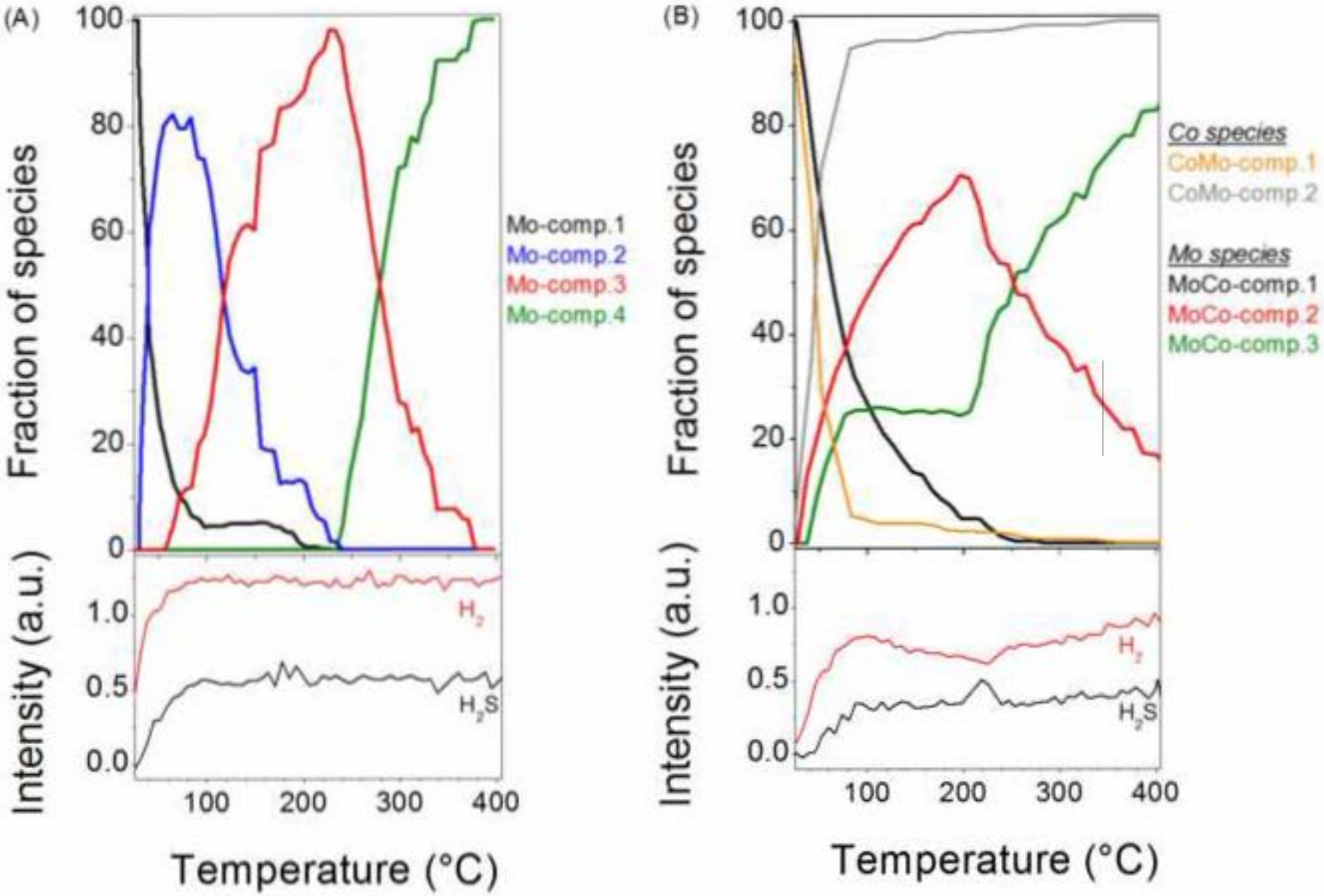

Figure 15

Click here to download high resolution image

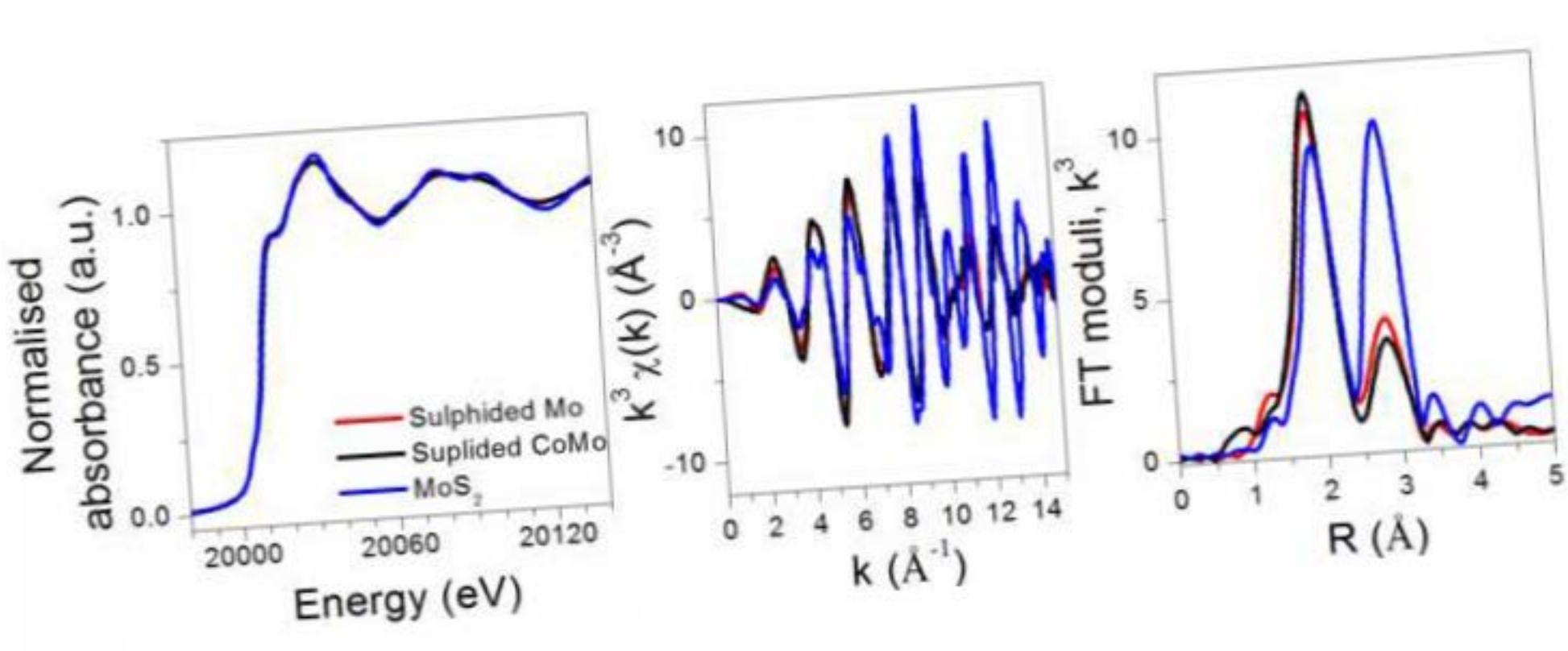

**Figure 16**

Click here to download high resolution image

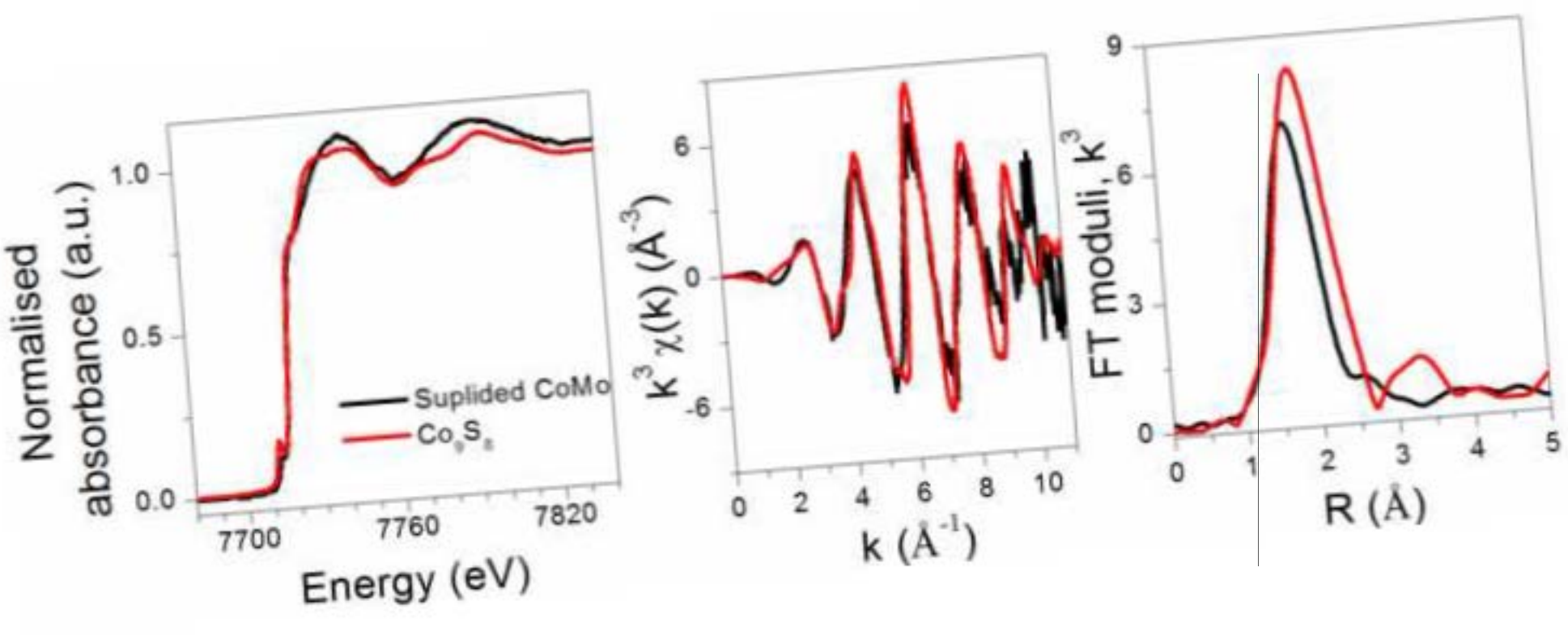

# Etude des propriétés de sulfuration de catalyseurs $Mo/Al_2O_3$ et $CoMo/Al_2O_3$ par spectroscopie d'absorption des rayons X résolue dans le temps aux seuils K du cobalt et du molybdène

# Co-K and Mo K edges Quick-XAS study of the sulphidation properties of $Mo/Al_2O_3$ and $CoMo/Al_2O_3$ catalysts

**Amélie Rochet[a,b,c,*], Bertrand Baubet[a], Virginie Moizan[a], Christophe Pichon[a], Valérie Briois[b,*]**

[a] IFP Energies nouvelles, Rond-point de l'échangeur de Solaize, BP 3, 69360 Solaize, France, 00 33 4 37 70 20 00, 00 33 4 37 70 27 45, virginie.moizan@ifpen.fr

[b] Synchrotron SOLEIL, L'Orme des Merisiers, Saint-Aubin, BP 48, 91192 Gif-sur-Yvette Cedex, France, 00 33 1 69 35 96 44, 00 33 1 69 35 94 56, valerie.briois@synchrotron-soleil.fr

[c] Laboratório Nacional de Luz Síncrotron, CEP 13083-970, Caixa Postal 6192, Campinas, São Paulo, Brazil, 00 55 19 35 17 51 80, 00 55 19 35 12 10 04, amelie.rochet@lnls.br

## Supporting Information

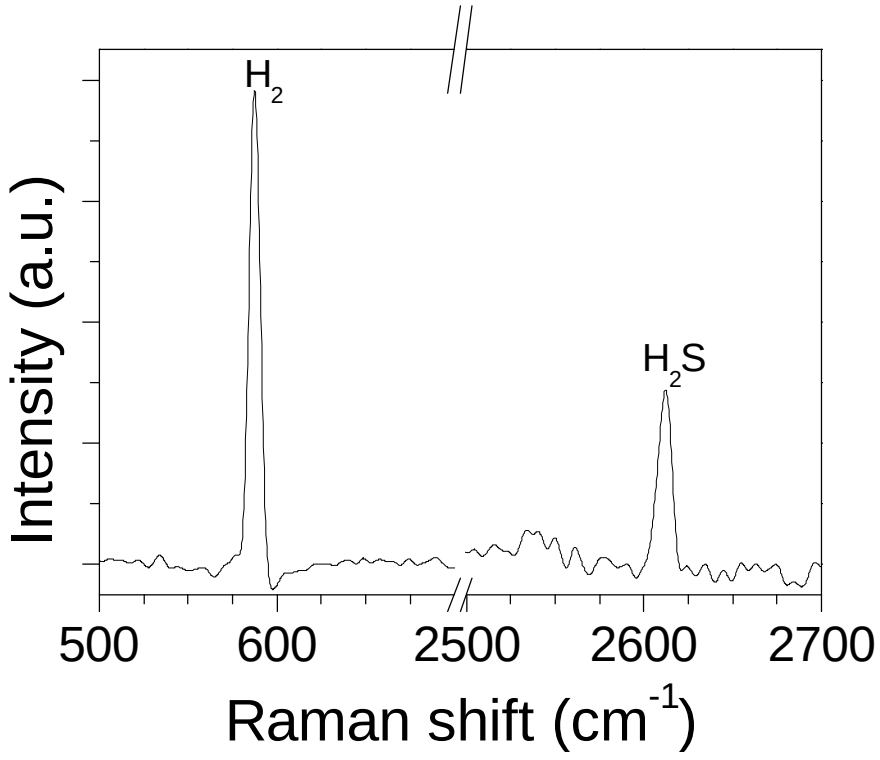


Figure S 1: Raman bands characteristics of $H_2$ and $H_2S$.

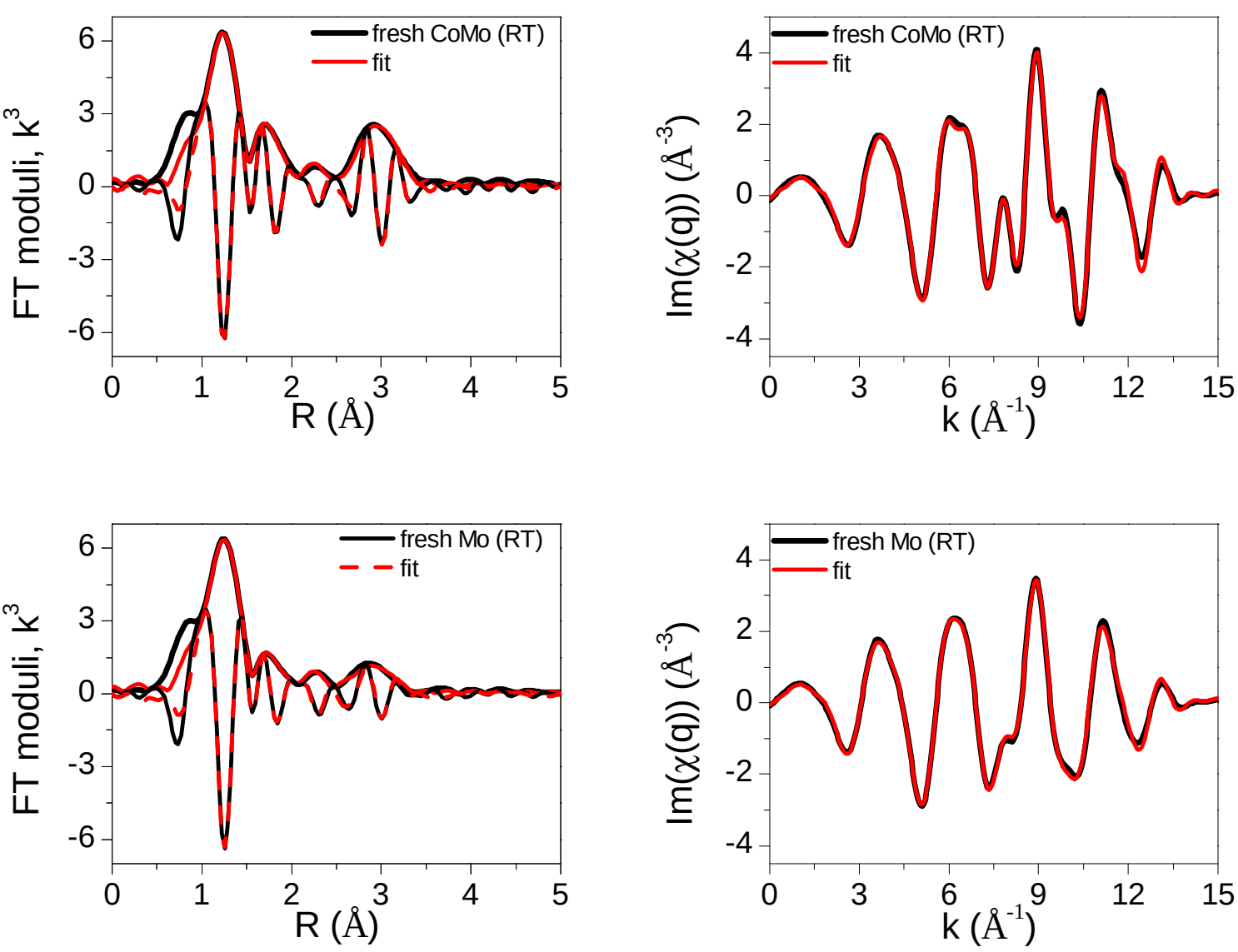


Figure S 2: Fitting of the Mo K edge EXAFS spectrum of the fresh bimetallic CoMo (top) and monometallic Mo (bottom) supported catalysts.

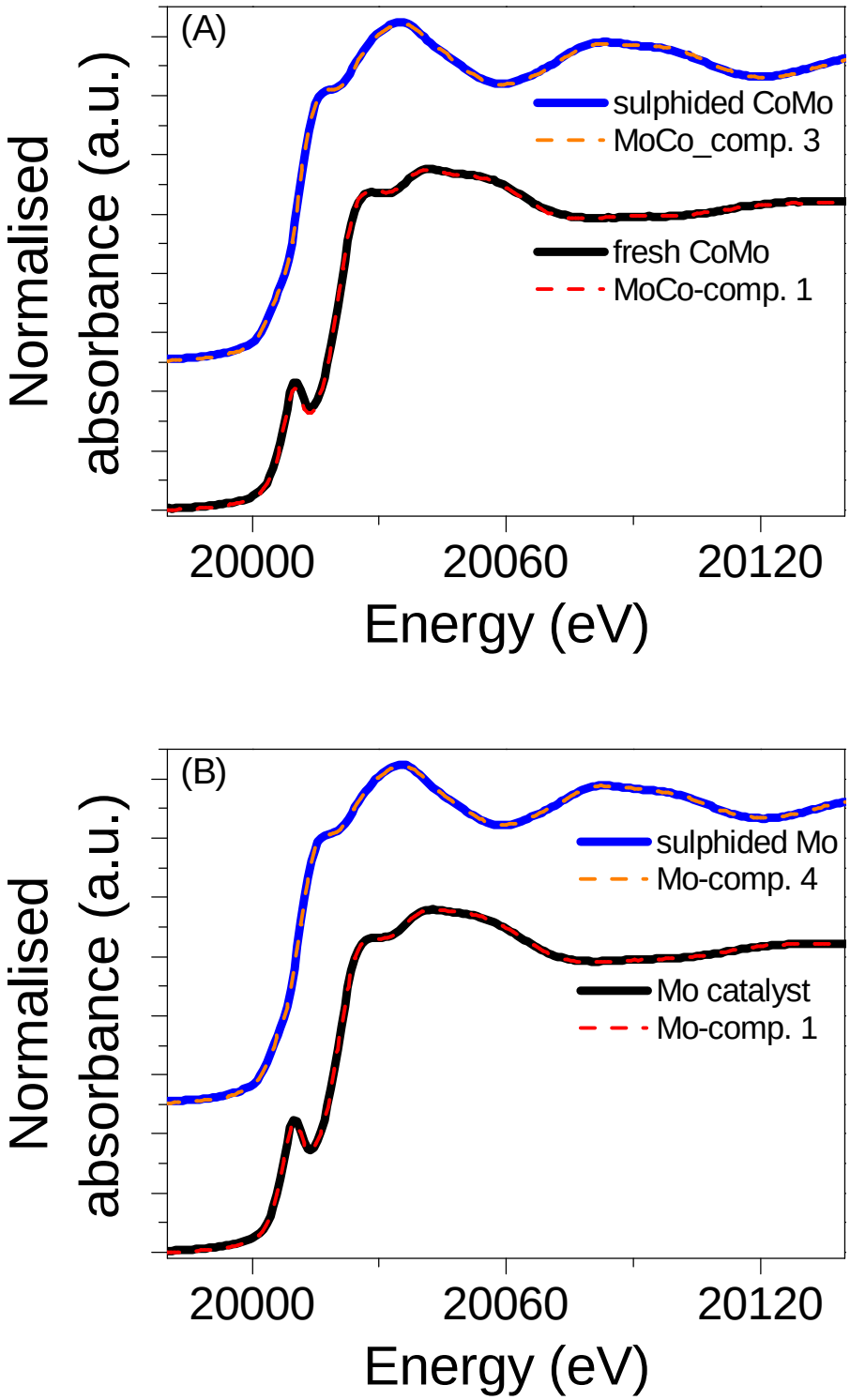


Figure S 3: Mo K edge XAS spectra of the first and last components determined by MCR-ALS compared to the fresh and sulphided catalysts for the bimetallic CoMo (A) and monometallic Mo (B) supported catalysts.

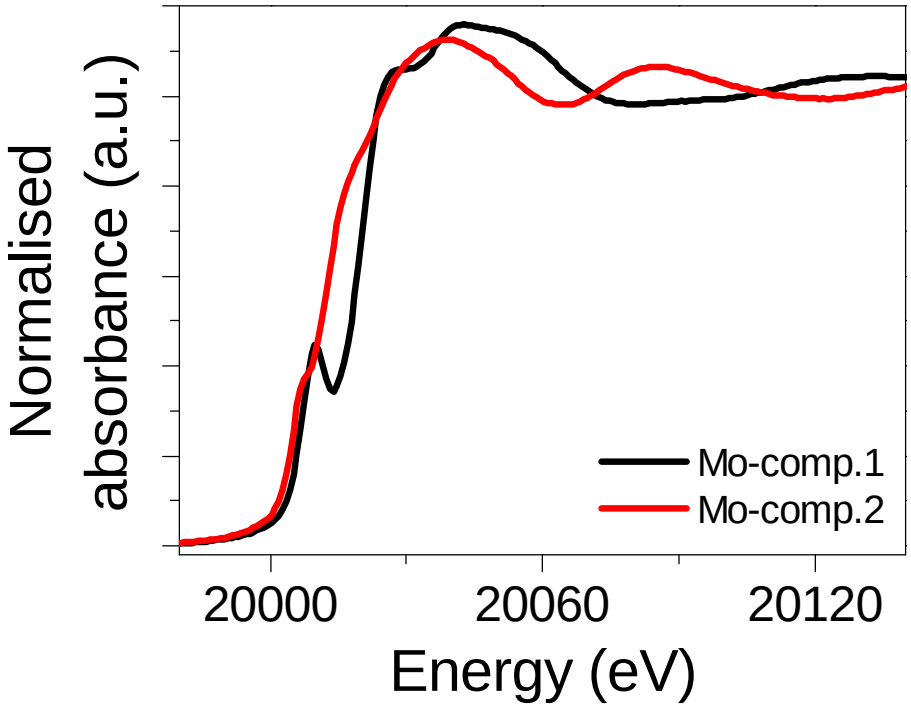


Figure S 4: Mo K edge XAS spectra of the first and second components determined by MCR-ALS for the monometallic Mo supported catalyst.

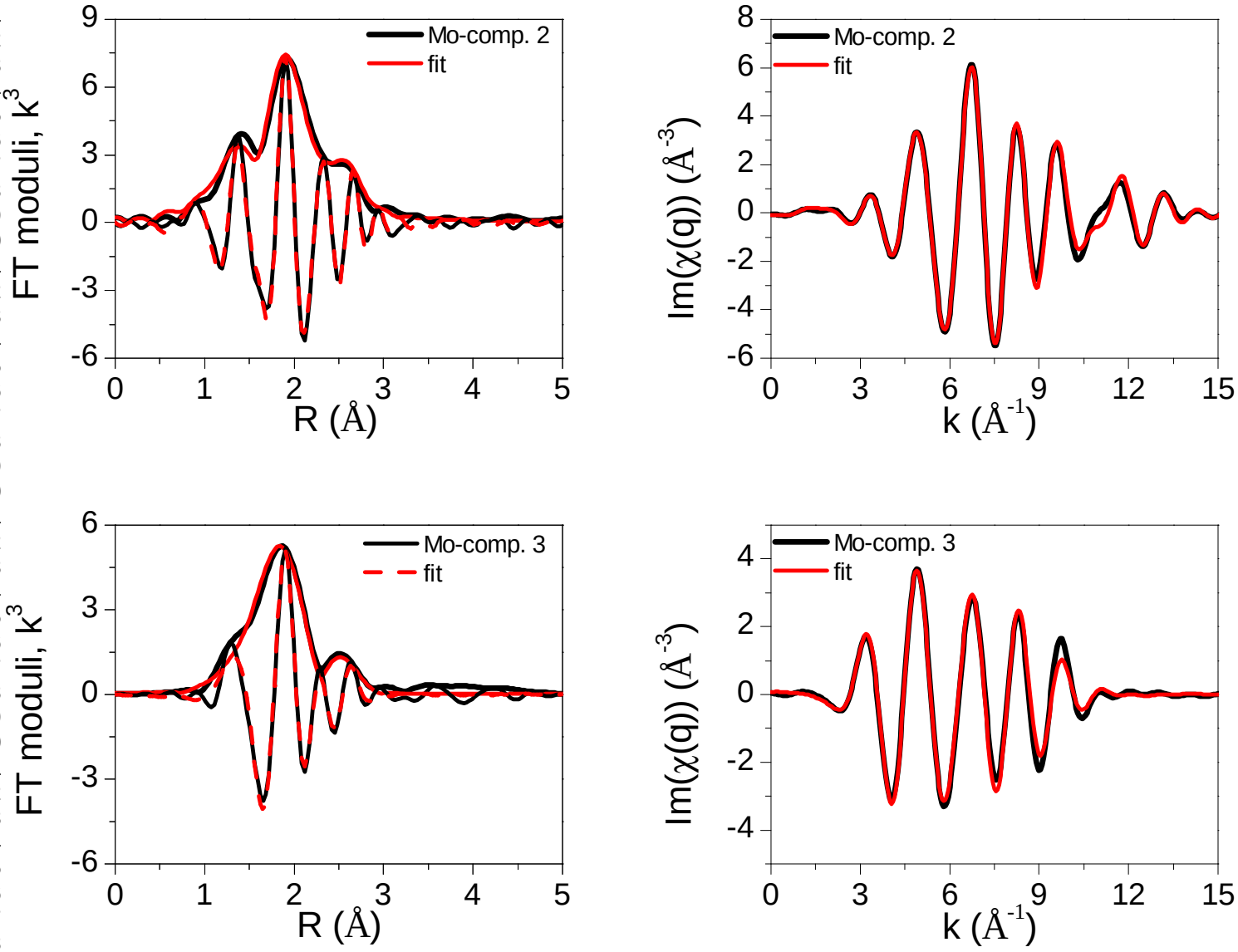


Figure S 5: Fitting of the Mo K edge EXAFS spectrum of the intermediate components *Mo-comp.2* (top) and *Mo-comp.3* (bottom) obtained by MCR-ALS of the monometallic Mo supported catalyst.

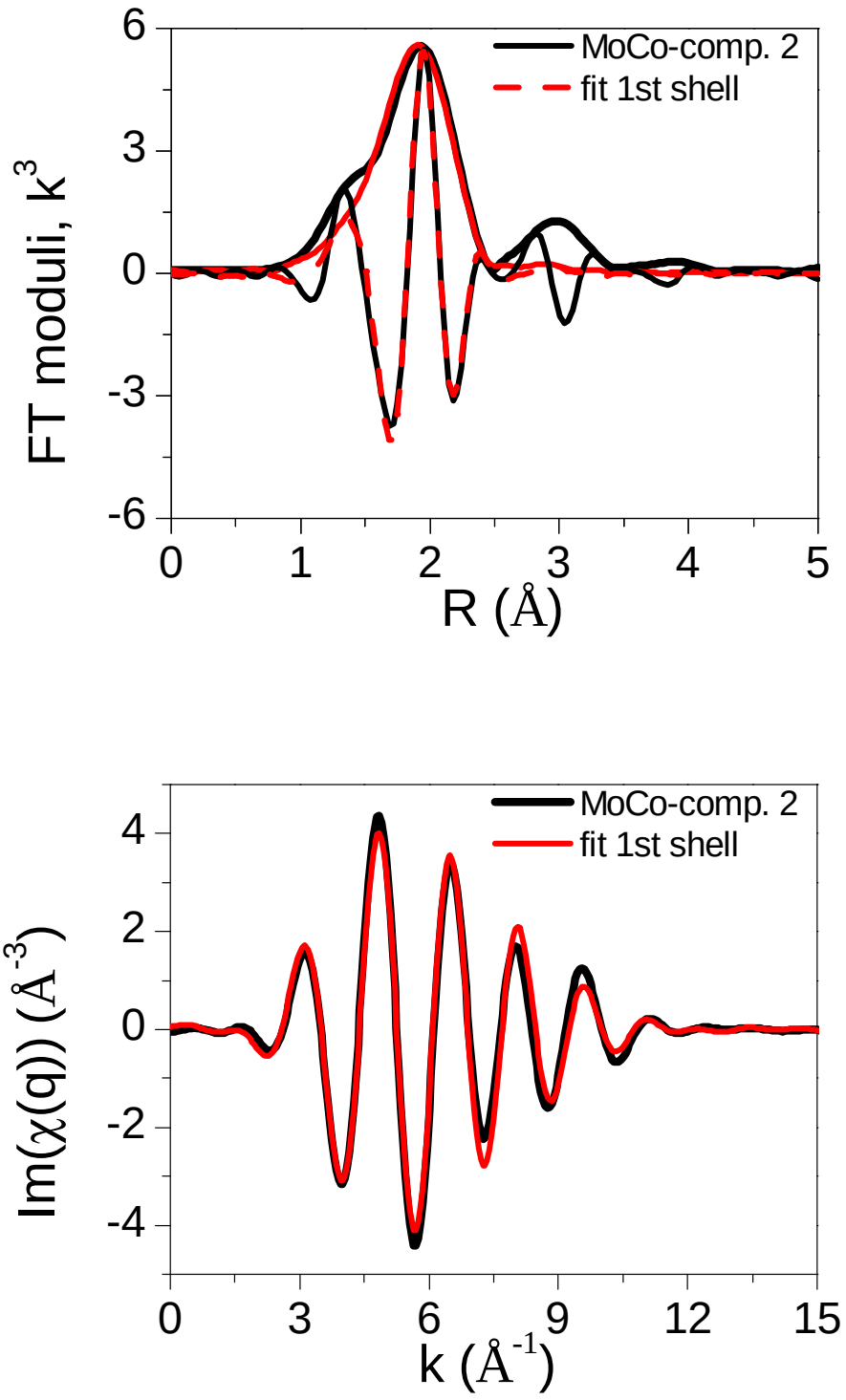


Figure S 6: Fitting of the Mo K edge EXAFS spectrum of the intermediate *MoCo-comp.2*.

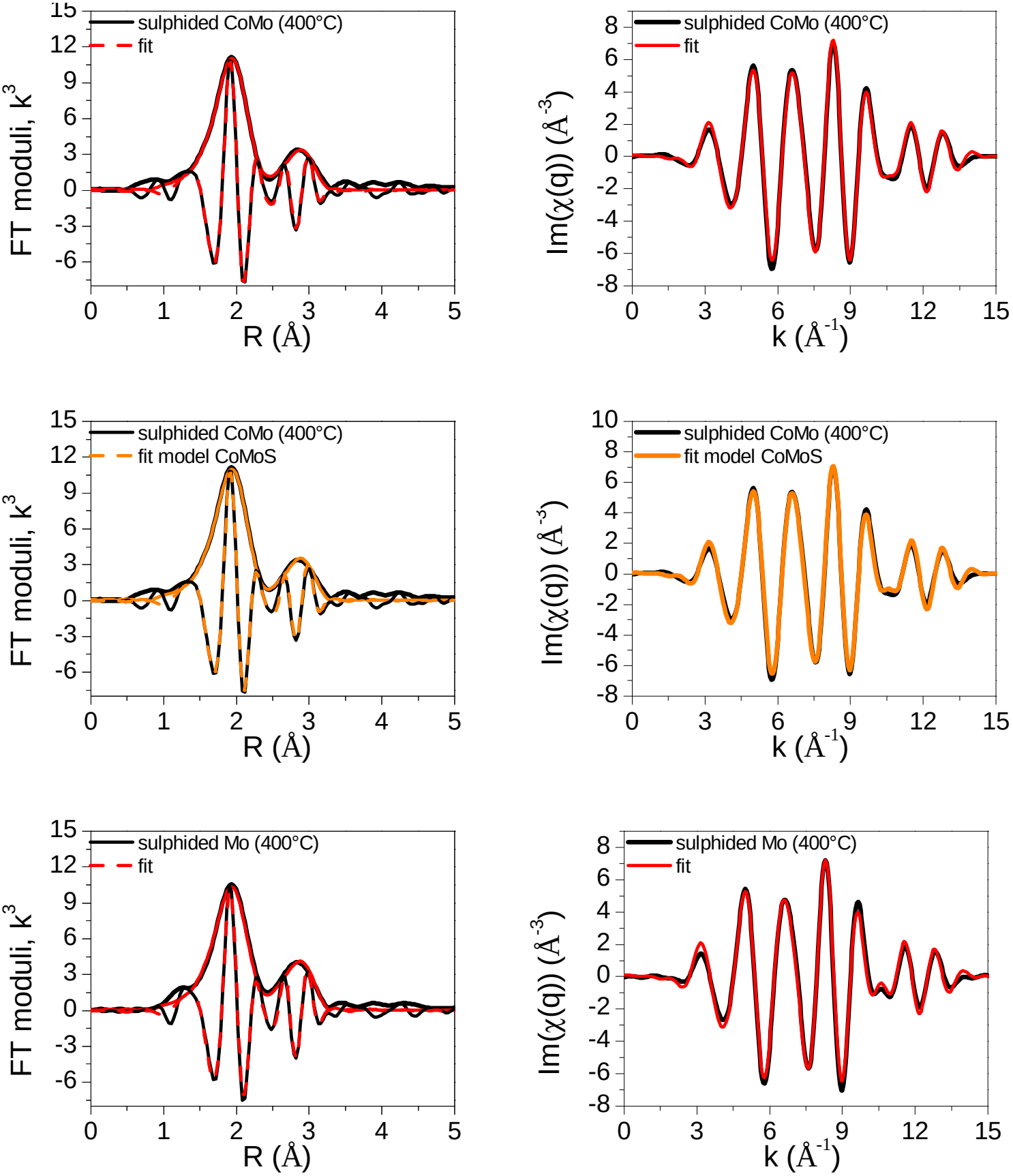


Figure S 7: Fitting of the Mo K edge EXAFS spectrum of the final sulphided bimetallic CoMo (top, middle) and monometallic Mo (bottom) supported catalysts.

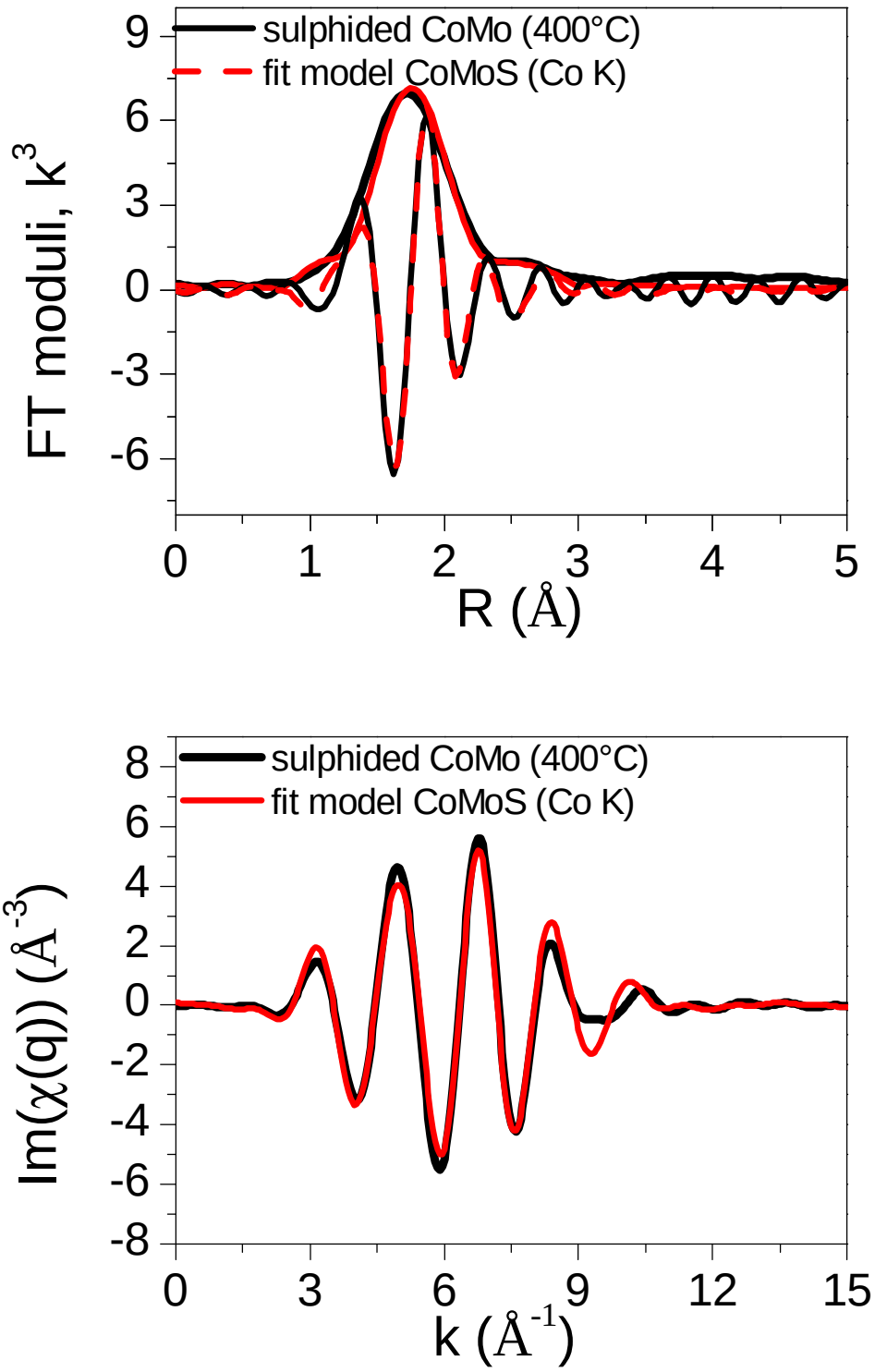


Figure S 8: Fitting of the Co K edge EXAFS spectrum of the final sulphided bimetallic $CoMo/Al_2O_3$ catalyst.